

Don't Get Me Wrong: How to Apply Deep Visual Interpretations to Time Series

Christoffer Löffler, Wei-Cheng Lai*, Björn M. Eskofier & Dario Zanca

Machine Learning and Data Analytics Lab

Friedrich-Alexander University Erlangen-Nuremberg

Carl-Thiersch-Straße 2b, 91052, Erlangen, Germany

{CHRISTOFFER.LOEFLER, WESLEY.LAI, BJOERN.ESKOFIER, DARIO.ZANCA}@FAU.DE

Lukas Schmidt† & Christopher Mutschler

Fraunhofer IIS, Fraunhofer Institute for Integrated Circuits IIS

Positioning and Networks Division

Erlangen, Germany

{LUKAS.SCHMIDT, CHRISTOPHER.MUTSCHLER}@IIS.FRAUNHOFER.DE

Abstract

The correct interpretation and understanding of deep learning models are essential in many applications. Explanatory visual interpretation approaches for image, and natural language processing allow domain experts to validate and understand almost any deep learning model. However, they fall short when generalizing to arbitrary time series, which is inherently less intuitive and more diverse. Whether a visualization explains valid reasoning or captures the actual features is difficult to judge. Hence, instead of blind trust, we need an objective evaluation to obtain trustworthy quality metrics. We propose a framework of six orthogonal metrics for gradient-, propagation- or perturbation-based post-hoc visual interpretation methods for time series classification and segmentation tasks. An experimental study includes popular neural network architectures for time series and nine visual interpretation methods. We evaluate the visual interpretation methods with diverse datasets from the UCR repository and a complex, real-world dataset and study the influence of standard regularization techniques during training. We show that none of the methods consistently outperforms others on all metrics, while some are sometimes ahead. Our insights and recommendations allow experts to choose suitable visualization techniques for the model and task.

Keywords: Deep Neural Networks, interpretable AI, explainable AI, visual interpretation, time series data, evaluation metrics

1. Introduction

Due to its high performance on complex multi-modal data, deep learning (DL) has become increasingly popular in many real-world applications that process time series data (Fawaz et al., 2019b). While we fundamentally rely on the networks' correct operation in many applications that consider safety (Berkenkamp et al., 2017) they remain difficult to interpret. Typical applications are the monitoring of industrial processes (Löffler et al., 2021), the support of healthcare and sports (Dorschky et al., 2020), or safety in autonomous driv-

*. With Friedrich-Alexander University Erlangen-Nuremberg when conducting this research.

†. With Fraunhofer Institute for Integrated Circuits IIS when conducting this research.

ing (Schmidt et al., 2021). The need for improved model understanding (Carvalho et al., 2019), along with regulatory guidelines (Goodman and Flaxman, 2017), led to a myriad of new approaches to the visual interpretation problem (Zhang and Zhu, 2018).

Post-hoc visual interpretation allows a domain expert to validate and understand how (almost) arbitrary deep learning models operate. Their central idea is highlighting features on the input that are "relevant" for the prediction of a learned model (Adebayo et al., 2018). Many of these techniques do not require a modification of the original model (Simonyan et al., 2014; Ribeiro et al., 2016), which makes them compatible with different architectures. Thus, they are helpful as a general-purpose validation tool for neural networks across different tasks (Arrieta et al., 2020).

However, while visual interpretation yields intuitive and correct explanations for images (Samek et al., 2021), the application of these methods on time series data is still a generally unsolved problem (Rojat et al., 2021). Time series are inherently more diverse (Rojat et al., 2021) because they may originate from various sensors and processes and often do not allow a prominent patch- or texture-based localization of critical features for human observers. Even though success is possible, e.g., when analyzing individual gait patterns Horst et al. (2019), applying and evaluating visual interpretability methods is difficult. A domain expert cannot easily judge if explanations are correct in (i) delivering the reasoning of the decision process in the DL model and (ii) capturing the actual features in the dataset that lead to a correct classification.

Hence, it is essential not to apply different visualization methods mindlessly. This requires quality metrics that evaluate visual interpretations and enable an expert to select a suitable visualization for a given model and task. However, both state-of-the-art visualization techniques and metrics that assess visual interpretations, e.g., Pixel Flipping (Samek et al., 2017), Sanity Check (Adebayo et al., 2018), and sensitivity checks (Rebuffi et al., 2020), so far have been examined on images (Rojat et al., 2021) or NLP tasks (Arras et al., 2017), but only rarely on more diverse time series (Schlegel et al., 2019). This lack of objective and subjective evaluation seriously limits their application and utility for time series.

This paper studies six orthogonal metrics that characterize the quality of visual interpretations for time series data. We investigate "sanity" (Adebayo et al., 2018), "faithfulness" (Melis and Jaakkola, 2018; Schlegel et al., 2019), "sensitivity" (Rebuffi et al., 2020), "robustness" (Yeh et al., 2019), "stability" (Fel and Vigouroux, 2020; Li et al., 2021a), and a novel metric based on annotations: "localization". These metrics rate and validate distinct qualities of saliency. We further investigate how training choices and conditions, like the dataset, model architecture, and regularization methods, modify the quality and characteristics of visual interpretations. Based on this investigation, we give clear recommendations that allow experts to choose and validate appropriate visualization methods for time series DL models.

In our extensive evaluation, we train four different architectures on two different types of tasks: U-Time (Perslev et al., 2019) and bidirectional Long Short-Term Memory (bi-LSTM) (Schuster and Paliwal, 1997) on segmentation tasks, and Fully Convolutional Network (FCN) (Long et al., 2015) and Temporal Convolutional Network (TCN) (Bai et al., 2018) on classification tasks. We use diverse datasets from the UCR repository (Dau et al., 2018) (GunPointAgeSpan, FordA, FordB, ElectricDevices, MelbournePedestrian,

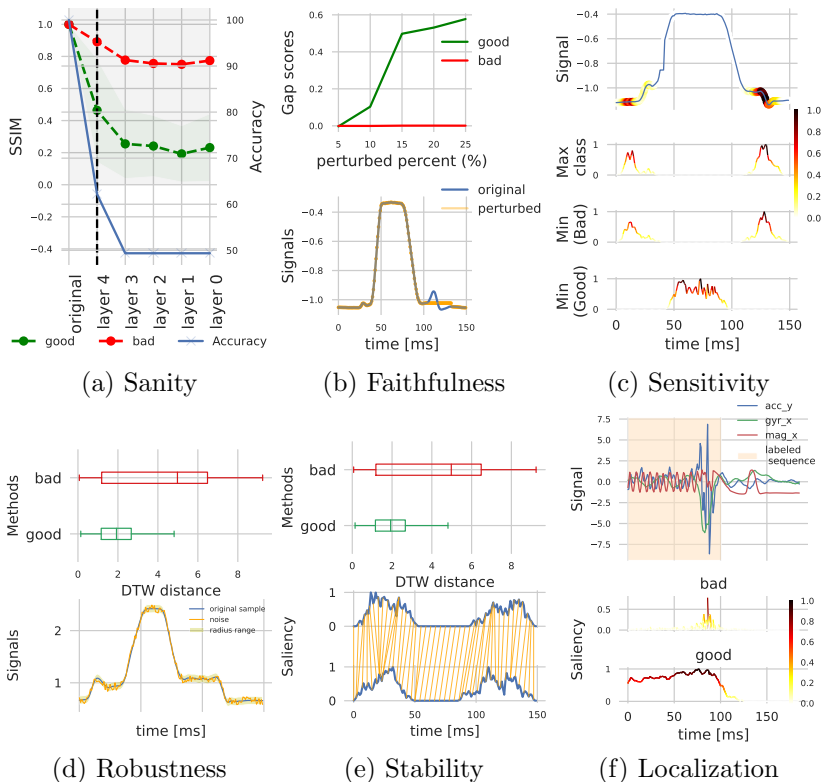


Figure 1: We show examples of a good (green) and a bad (red) score for each metric: (a) sane saliency depends on network parameters, tested by randomizing weights and biases; (b) faithful saliency correlates with predictive accuracy, tested by perturbing the input sequence; (c) sensitive saliency of the predicted class in one sample is different from others; (d) for robust saliency small changes to input data cause only small effects; (e) stable saliency assigns relevance to similar features for the same class; (f) saliency should be localized on the predicted segment.

NATOPS) for classification and the more complex real-world tool tracking dataset (Löffler et al., 2021) for segmentation. Additionally, we evaluate the effects of dropout and ℓ_1 - and ℓ_2 -regularization. The experiments show the necessity of all categories to create an objective rating for methods, models, and tasks and highlight the importance of the regularization technique during model training. Our recommendations help domain experts understand, rate, and validate saliency for time series in safety-critical applications.

The remainder of this article is structured as follows. Section 2 discusses background and related work. Section 3 introduces extended and novel metrics for classification and segmentation tasks. Section 4 discusses our experimental results. Based on these findings, Section 5 proposes recommendations. Section 6 concludes.

2. Background and Related Work

Interpretation methods for DL models can be divided into ante-hoc methods, which are inherently part of the model, and post-hoc methods, which provide the interpretation after training (Rojat et al., 2021). We focus on post-hoc techniques and divide them into gradient-, propagation- and perturbation-based methods (Li et al., 2021a; Warnecke et al., 2020; Ismail et al., 2020; Letzgus et al., 2022).

Gradient-based methods compute the relevance for all input features by passing gradients backward through the neural network (Baehrens et al., 2010). *Gradient* (Simonyan et al., 2014) computes the saliency map M^c of a class c using the derivative of the class score P^c of the model with respect to the input sample x , as $M^c(x) = \frac{\partial P^c}{\partial x}$. The gradient indicates the importance of points in the input sequence for predictions. The advantage of gradient-based methods lies in their computational efficiency, as they use only a small number of backward passes to compute $M^c(x)$.

Propagation-based methods leverage the network’s structure to produce the explanation (Letzgus et al., 2022). They propagate the output predictions back to the input. Methods such as Layerwise Relevance Propagation (LRP) (Bach et al., 2015) implement propagation rules for different layer types. LRP computes relevance R_j at layer j based on the contributions from the relevance R_k of the consecutive layer at index k . Let Z_{jk} denote the forward pass contribution of neuron j to neuron k . LRP then sums over previous contributions $\sum_{0,j}$ and current contributions \sum_k to get the relevancy $R_j = \sum_k \frac{Z_{jk}}{\sum Z_{jk_0,j}} R_k$. We refer to Letzgus et al. (Letzgus et al., 2022).

Perturbation-based methods perturb known input samples and measure the effects of specific perturbations on the predicted class via a forward pass through the network. For instance, Local Interpretable Model-Agnostic Explanations (LIME) (Ribeiro et al., 2016) fits a local surrogate model (e.g., a linear regression) as an explanation and calculates relevance based on this surrogate. Perturbation-based methods are computationally expensive as they require multiple forward passes per sample. However, they do not need gradient information and work with black-box models.

2.1 Metrics for Saliency on Time Series

Most interpretation methods were originally designed for image or text data. Compared to more abstract time series, understanding and comparing visual interpretation is intuitive on image data. Furthermore, the diversity of interpretation methods complicates an objective choice for the model and task (Rojat et al., 2021). For example, when Wang et al. (2017) and Fawaz et al. (2019b) apply Class Activation Maps (CAM) (Zhou et al., 2016) on well-known UCR datasets (Dau et al., 2018), they notice a qualitative difference of CAM interpretations between network architectures. This suggests that the difference in quality should be quantified. Similarly, other work relies on domain experts that perform a (costly) qualitative evaluation that is costly compared to an algorithmic one (Strodthoff and Strodthoff, 2019; Fawaz et al., 2019a; Oviedo et al., 2019). Hence, there is an increasing need for objective evaluation metrics to make the interpretations’ quality measurable and comparable.

2.2 Categories of Metrics

Relying on only one saliency metric to interpret a model’s behavior could be misleading (Tomsett et al., 2020). This leads to the question of how users should evaluate saliency methods (Li et al., 2021a), and what questions the saliency metrics should answer (Doshi-Velez and Kim, 2017; Silva et al., 2018; Carvalho et al., 2019). Doshi-Velez and Kim (2017) distinguishes saliency metrics as either human-grounded or functional metrics. Human-grounded tests may assess whether an explanation can be quickly understood by a human (Doshi-Velez and Kim (2017); Li et al. (2021a)), or ask humans about their opinion on the quality of explanations (Li et al., 2021a). However, since they require humans, they are costly to scale (Li et al., 2021a). In addition, human-grounded methods, such as using bounding boxes for the expected location of saliency (Jianming et al., 2016) can disregard whether saliency methods correctly capture model behavior. They may hide spurious correlations (e.g., ”clever Hans” samples Lapuschkin et al. (2019); Li et al. (2021b); Anders et al. (2022)). Functional metrics do not involve humans but provide statistical measures that aim to capture actual model behavior, e.g., to aggregate performance metrics automatically (Rojat et al., 2021), and use proxy tasks to generate a quantitative evaluation. Furthermore, the recent quantitative study on image data conducted by Li et al. (2021b) confirms Tomsett et al. (Tomsett et al., 2020) and extends the notion that even with a set of saliency metric no saliency method dominated the others.

Unlike prior work, this article proposes a metrics framework with orthogonal categories, specifically for time series. We adapt and extend metrics to (multivariate) time series and propose an intra-class stability metric and a concept of relevance localization: we build on the pointing game (Jianming et al., 2016) and combine it with the precision and recall for time series (Tatbul et al., 2018). Furthermore, we provide an in-depth evaluation and discussion of saliency methods and confirm the influence of regularization on time series classification.

3. Scoring Categories

We propose six distinct categories (”sanity”, ”faithfulness”, ”sensitivity”, ”robustness”, ”stability”, and ”localization”) to assess visual interpretation methods and to determine their performance and trustworthiness in classification or segmentation tasks on time series. For each of them, we propose a metric that enables a comparative evaluation of diverse visual interpretation methods.

Why do we need six scoring categories? It seems tempting to rely on a single metric or aggregated score across multiple metrics to assess the quality of a visual interpretation. However, we show that our six presented categories are orthogonal (see Fig. 2) and capture distinct attributes. This finding also confirms previously discussed studies Li et al. (2021b); Tomsett et al. (2020). It extends work by Hedström et al. (Hedström et al., 2023), who loosely cluster quantitative evaluation metrics into six groups based on their intuitive similarity¹. Interpretations depend on model parameters (sanity check (Adebayo et al., 2018)), predictive features (faithfulness (Melis and Jaakkola, 2018)), coherence of class predictions (intra-class stability (Fel and Vigouroux, 2020)), robustness against noise (max

1. parallel work, see our preprint <https://arxiv.org/abs/2203.07861>

sensitivity with adversarial noise (Yeh et al., 2019)), specific sequences (or even points) in a time series like by Tatbul et al. (2018) (novel localization metric), and the relevance map’s specificity (inter-class sensitivity (Rebuffi et al., 2020)). It is crucial to assess if a given interpretation accurately captures these dependencies.

We briefly overview our metrics in Fig. 1. As a set, they allow in-depth analysis of saliency methods performance on time series data while still being independent, see also Sec. 5 for details.

- (a) *sane saliency* depends on network parameters and is structurally different after randomizing the network’s weights ρ_i for layers [1, 2, 3] (Adebayo et al., 2018).
- (b) *faithful saliency* correlates with predictive accuracy. Perturbing a percentage of the input sequence with high saliency decreases accuracy (Melis and Jaakkola, 2018).
- (c) saliency is *sensitive* if the predicted (max) class in one sample is sufficiently different from any other (min) class (Rebuffi et al., 2020).
- (d) saliency is *robust* if small changes to the input cause only small changes to the saliency (Yeh et al., 2019).
- (e) saliency is *stable* if it assigns relevance to similar features for all samples of a class, wrt. a suitable distance metric (Fel and Vigouroux, 2020).
- (f) saliency should be *localized* on the segments of the predicted classes (t_0 to t_1).

Faithfulness TI	1	0.1	0.1	-0.16	0.35
IC. Stability	0.1	1	0.25	-0.24	-0.13
Robustness	0.1	0.25	1	-0.2	0.11
Sanity	-0.16	-0.24	-0.2	1	0.028
Sensitivity	0.35	-0.13	0.11	0.028	1
	Faithfulness TI	IC. Stability	Robustness	Sanity	Sensitivity

Figure 2: Pairwise Pearson correlations of scores. Every metric is independent of all others.

Notation. We first introduce a unified notation that we adapt from Fawaz et al. (2019b): A multivariate time series is defined by $X = [X^1, \dots, X^H]$, where H is the number of input channels, $X^i = (x_1^i, \dots, x_T^i) \in \mathbb{R}^T$ is an ordered set of real values, and T denotes the number of time steps. For $H = 1$, we consider a *univariate* time series; otherwise, we consider a *multivariate* time series. Time series often include complex temporal dependencies, i.e., distinct points are not independent. Time series classification defines a mapping $X \rightarrow y$ that minimizes the error on a dataset $D = \{(X_1, y_1), \dots, (X_N, y_N)\}$, where N is the number of data samples, $X \in D$ is a time series, $y_i \in \mathbb{R}^C$ denotes the one-hot vector of a class label the input belongs to, and C is the number of classes. In time series segmentation, we search $X \rightarrow Y$ that maps an input sample to a dense classification $Y = [y_1, \dots, y_T] \in \mathbb{R}^{C \times T}$ (Perslev et al., 2019), i.e., a class label is predicted for each time step. Post-hoc visual interpretation methods compute a relevance map $M_m^c \in \mathbb{R}^{H \times T}$, $M_m^c(X) = [R^1, \dots, R^H]$, where $R^i = (r_1^i, \dots, r_T^i)$, representing the importance of each input feature wrt. the class c and a model m , for each time step. We use M as a function to

produce the saliency map. For clarity, we will omit the dependency on m , i.e., $M_m^c \equiv M^c$, if it is not explicitly required. An evaluation metric for visual interpretation methods defines a score $\mathcal{S}_{\text{metric}}(\cdot)$ that rates the quality of the relevance map M at a sample X given a model m and optional parameters. We provide a unified view so that for all scores, a higher score corresponds to a better visualization according to the perspective.

3.1 Sanity

The sanity metric measures the idea that a visual interpretation depends on the interpreted model. Intuitively, suppose the weights and biases of a trained network model were re-initialized with random values. The network’s predictions and generated saliency maps should also differ from the original maps. However, this is not always the case. Despite a drop in model accuracy, saliency may remain stable. Hence, we test sanity using a variant of sanity checks proposed by Adebayo et al. (Adebayo et al., 2018), that performs a *layer-wise cascading randomization* of the network’s weights and biases, starting from the output to the input. In contrast to independent randomization, the cascading approach results in a mostly continuous performance degradation of predictions, see Fig. 1a for an illustration. Network accuracy should increasingly resemble a random guessing. Following Adebayo et al. (2018), we compare saliency using the structural similarity index measure (SSIM) (Wang et al., 2004), which compares the distribution of sub-sequences of M^c . We define the sanity score as

$$S_{\text{Sanity}}(M, D, m) = -\frac{1}{N} \cdot \sum_{X \in D} \sum_{i=1}^L \frac{\text{SSIM}(M_m^c(X), M_{m_i}^c(X))}{L}, \quad (1)$$

where $|D| = N$, i enumerates the L layers of m , whose parameters are randomized and $M_{m_i}^c(x)$ is the saliency map after randomizing layer i of m . We average the SSIM over L layers and compute the average over all samples in D .

More recently, Yona and Greenfeld Yona and Greenfeld (2021) demonstrated that this variant of sanity checks is distribution-dependent and cannot exclusively be relied on when comparing saliency methods. However, the authors do not challenge the sanity checks idea and use it for debugging or explaining models. Hence, we integrate them as one of six perspectives into our framework.

3.2 Faithfulness

A relevance measure is faithful if input features with a high relevance (w.r.t. M^c) have a high influence on the model prediction, see Fig. 1b for an illustration. Melis and Jaakkola (2018) propose a perturbation-based metric that evaluates the faithfulness of predictions. The metric measures the correlation between input (features) with high saliency on the one hand and predictive accuracy on the other hand. For time series data, two variants of faithfulness are based on different data distribution assumptions. Both rank inputs of the time step of $X_T \in \mathbb{R}^T$ according to the relevance of its saliency map. However, they differ in perturbations: Melis and Jaakkola (2018) (further called Temporal Importance (TI)) strictly adhere to the ranked importance of saliency to choose what to perturb. In contrast, Schlegel et al. (2019) assume temporal correlation of inputs and perturb a connected sub-sequence instead (Temporal Sub-sequences (TS)). While the latter is a more intuitive model for perturbations on time series data, it may misrepresent the importance of features, e.g.,

if they are not clustered or do not follow the assumption that they should be sequential. Furthermore, there may be several crucial sub-sequences in a single sample.

We use either variant of faithfulness on multivariate data X_T^H as follows. Based on the relevance r , we select time points $t \in \{1, \dots, T\}$ and features $i \in \{1, \dots, H\}$. For TI, we select and perturb the inputs of the sample X with the highest relevance r_t^i and replace their values with the data’s mean at time t , as proposed by Melis and Jaakkola (2018). For TS, we select t according to the maximum relevance r_t^i and perturb a sub-sequence of the inputs of the sample X by replacing its values also with a mean value of the data of length L at time t , as $x_{\text{mean}} = (x_{t+\frac{L}{2}}^i, \dots, x_t^i, \dots, x_{t-\frac{L}{2}}^i)$, to break the temporal correlation, following Schlegel et al. (2019). We choose to perturb samples with mean values, making it less likely to move them off their manifold Montavon et al. (2018).

The perturbed sample is denoted as X' . We compute the mean faithfulness scores over the whole dataset D for TI as

$$S_{\text{Faithfulness TI}}(M, D, m) = -\frac{1}{N \cdot L} \sum_{X \in D} \sum_{l=0}^L m^c(X'_l) \quad (2)$$

and for TS, as

$$S_{\text{Faithfulness TS}}(M, D, m) = \frac{1}{N} \cdot \sum_{X \in D} m^c(X) - m^c(X'), \quad (3)$$

where $m^c : R^c \rightarrow R$ is the softmax prediction of the target class c . For TS, the gap score between the softmax prediction of the original and the perturbed sample is $m^c(X) - m^c(X')$. For TI, we use the Area Under Curve (AUC) instead, where L is the total perturbation length and X'_l is the perturbed sample at step l .

It is crucial to be aware of metrics’ biases when interpreting the scores of either TS or TI. Faithfulness implementations implicitly favor the saliency method that aligns well with the metric’s computation Covert et al. (2021), i.e., TS favors sub-sequences. In contrast, TI avoids this, and practitioners should pick the most suitable one depending on the use case.

3.3 Inter-Class Sensitivity

In multi-class prediction tasks, the classifier must identify relevant features for each class to make a correct prediction. Hence, the relevance map M^c should identify different salient features for those different classes (Li et al., 2021a), see Fig. 1c. If a method is not sensitive to the class, the score may indicate that the saliency is misleading or that the classifier failed to learn the correct features for these classes, and the sensitivity score should raise a red flag. Following Rebuffi et al. (2020), we assume that the class with the highest predicted probability is salient, and the one with the lowest confidence is uninformative because it is not contained in the sample. Taking the least confident class thus avoids (semantically) similar samples to be picked, which may well occur in large enough datasets with overlapping categories. Concretely, inter-class sensitivity (Rebuffi et al., 2020) measures class-specific sensitivity of the generated relevance map for the most likely (c_{max}) and least likely (c_{min}) class according to the model. We compute the mean inter-class sensitivity score as

$$S_{\text{Inter-Class Sensitivity}}(M, D) = -\frac{1}{N} \cdot \sum_{X \in D} \text{sim}(M^{c_{\text{max}}}(X), M^{c_{\text{min}}}(X)). \quad (4)$$

We compute similarity of two saliency maps as $\text{sim}(M^{c_{\text{max}}}(x), M^{c_{\text{min}}}(x))$ where $\text{sim}(\cdot, \cdot)$ is a similarity function (e.g., a cosine similarity) that is easy to interpret via its geometric

interpretation. It is defined as the angle between two non-zero vectors that measures the similarity between their inner product space (Han et al., 2012). Similarity of M in binary classification would result in a negative cosine similarity, meaning nearly inverted saliency maps for max- and min-classes.

The sensitivity of the saliency map is not always strictly related to how well the saliency method captures model behavior. Saliency methods of low faithfulness could introduce their bias to the sensitivity score and hide actual model behavior. However, inter-class sensitivity is still a helpful indicator of the quality of a model and visualization, with the important caveat that a score is only meaningful if the visualization is both faithful and sane. See Section 5 for further details and recommendations on this.

3.4 Robustness

Saliency methods may be vulnerable to small input changes and even adversarial attacks Dombrowski et al. (2019, 2022). For reliable interpretations, saliency methods should be as robust to small changes in the input as the model itself. We evaluate a method’s robustness to noise via its sensitivity of the most likely class (c_{\max}) as proposed by Yeh et al. (Yeh et al., 2019), see Fig. 1d for an illustration. Intuitively, even with noisy inputs, the saliency map of a model should not change significantly (Alvarez-Melis and Jaakkola, 2018), meaning that saliency maps with high sensitivity are less reliable. Yeh et al. (2019) define the sensitivity of the saliency map derived from the gradient as

$$[\nabla_X M^c(X)]_j = \lim_{\epsilon \rightarrow 0} \frac{M^c(X + \epsilon e_j) - M^c(X)}{\epsilon} \quad (5)$$

for any $j \in \{1, \dots, |H \cdot T|\}$, where $e_j \in \mathbb{R}^{H \times T}$ is the j -th coordinate vector and the j -th entry is one while the others are zero. We use Monte Carlo sampling of ϵe_j , where $|\epsilon e_j| < a$ (a is a user-specified radius), to generate different $\hat{X} = X + \epsilon e_j$. We compare \hat{X} with the original X to compute

$$S_{\text{Max Sensitivity}}(M^c, D, a) = -\frac{1}{N} \cdot \sum_{X \in D} \max_{\|\hat{X} - X\| < a} \|M^c(\hat{X}) - M^c(X)\|. \quad (6)$$

Alvarez et al. question whether saliency methods should be robust when the underlying model is not (Alvarez-Melis and Jaakkola, 2018), i.e., if an explanation should include noisy pixels (in image processing). They reason that pixel-exact saliency is helpful for exact debugging, while stable aspects are more valuable for understanding the predictor and the underlying phenomenon. Alternatively, Agarwal et al. (2022) proposed relative stability metrics that measure the changes in output explanation w.r.t. a white box model’s learned representations. In summary, especially if the underlying models are not robust, the robustness of saliency methods and models should be jointly evaluated and studied further.

3.5 Intra-Class Stability

Two explanations of the same feature should be similar, independent of their exact location within the input sample. This is helpful for generalization, as features may be translation-invariant, and predictors should point out the same evidence across samples of the same class Fel et al. (2022). Fel et al. (2022) propose algorithmic stability measures to

test whether saliency methods produce similar interpretations for samples from the same class.

To compute this metric, we need to make several assumptions. First, we assume that the order of temporal features is correlated between different samples of the same class. This is a reasonable assumption since time series data often contains distinct temporal features that follow a dataset-specific order. However, note that scores for intra-class stability are highly dataset-specific and should not be compared across different datasets. See Fig. 4 for this evaluation. Second, we assume that the visualization method is faithful and that both the visualization and the model are robust. This assumption must be validated for every model and visualization technique combination.

Based on these assumptions, we can test the intra-class stability of saliency maps M^c for a given dataset D using distance statistics, see Fig. 1e for an illustration. Specifically, we compute pairwise distances between saliency maps M^c for different samples $X_i, X_j \in D$ and aggregate these across classes:

$$S_{\text{Intra-Class Stability}}(M^c, D) = - \sum_{i \in [0, N]} \sum_{j \in [i+1, N]} \frac{d_{\text{dtw}}(M^c(D_i), M^c(D_j))}{N \cdot (N-1)}. \quad (7)$$

We use Dynamic Time Warping (DTW, Vintsyuk (1968)) as the distance function d_{DTW} to account for the time series nature of the data. The score compares each class’s sample’s M^c with all other samples’ saliency maps in the dataset, using d_{DTW} . DTW provides a crucial benefit by comparing time series with similar features in the same causal order but not simultaneously. In contrast, Fel et al. (2022) evaluate saliency methods’ generalization through algorithmic stability. They train two predictor models on different folds, i.e., datasets with and without the sample X , and only then compare the predictors’ saliency on the X .

3.6 Localization

The temporal location of class-specific features with high relevance in a time series segmentation task should intuitively be situated within (or close by) its labeled segment (temporal sub-sequence). This labeled sequence should also determine the location of saliency for models, see Fig. 1f for an illustration. Localization is a novel metric that measures this notion and allows experts to uncover potential problems in model operations like shortcut learning.

Similar to intra-class stability, localization requires a faithful visualization. Additionally (but somewhat obviously), accurate labels are needed to compute a meaningful score. Given a faithful visualization, samples with lower scores (lower overlaps) warrant closer inspection. A low localization score indicates spurious correlations due to unexpected features outside the labeled sequence and can also help pinpoint faulty labels.

Our metric extends the Pointing Game (Jianming et al., 2016) metric, previously used for object detection, to time series using range-based metrics (Tatbul et al., 2018). Localization systematically analyzes the saliency maps’ ranges in segmentation tasks. We argue that Pointing Game’s original hit-and-miss accuracy is inadequate for time series methods, as segmentation is point-wise exact. Thus, we replace it with range-based testing, yielding localization. This extension with front, middle, and back biases can help uncover problematic issues such as temporal biases within the labeled sub-sequence or the labels’ im-

precise margins. Furthermore, the metric may hint at learned shortcuts outside the labeled sequence.

We compute localization as follows. First, we filter out non-relevant predictions (according to the relevance map). A prediction at time t , denoted with $\hat{Y}(t)$, is relevant if there exists an $i \in \{1, \dots, M\}$ such that $r_t^i > \max(|r|) \cdot \theta$ where θ is a value between $[0, 1]$. We select the model’s predicted class at time t if the prediction is relevant. Otherwise, we set the class to *none*. The resulting *relevancy-filtered* prediction is denoted as \hat{Y}' . Finally, we can compare \hat{Y}' with the ground truth Y and evaluate how well high saliency features lie within the annotated sub-sequences (Tatbul et al., 2018).

To compute the mean localization score for the whole dataset D , we compare any of the N_{sub} existing labeled sub-sequence $Y_{\text{sub}_i} \in R^T$ from D each with its temporally co-located prediction \hat{Y}'_i

$$S_{\text{localization}}(Y, \hat{Y}') = \sum_{i=0}^{N_{\text{sub}}} \frac{S_{\text{recall}}(Y_{\text{sub}_i}, \hat{Y}'_i)}{N_{\text{sub}}}. \quad (8)$$

For each pair $(Y_{\text{sub}_i}, \hat{Y}'_i)$ we calculate a range-based recall score based on the point-wise comparison proposed by Tatbul et al. (2018) as

$$S_{\text{recall}}(Y_{\text{sub}}, Y') = \alpha \cdot \text{existence}(Y_{\text{sub}}, Y') + (1 - \alpha) \cdot \text{overlap}(Y_{\text{sub}}, Y'), \quad (9)$$

where α weighs the two reward terms for "existence" and "overlap". Existence is 1 if any time point was correctly predicted within the labeled region and 0 otherwise. The parameterized "overlap" function determines the finer properties of cardinality, size, and position. The cardinality parameter discounts the score if the prediction is an interrupted and fragmented range instead of continuous. The predicted and label ranges’ overlap size depends on a positional bias. It may favor "front", "middle", or "back" overlap. Practically, for some applications, early detection is preferable over late detection. Salient features outside the labeled range Y_{sub_i} can be scored analogously simply by inverting the range. For further details, see Appendix A or Tatbul et al. (2018).

4. Experiments

Our experiments show a representative evaluation of the presented framework for the diverse field of time series. A broad evaluation is also necessary because saliency methods’ explanations may be highly data-dependent. Kindermans et al. Kindermans et al. (2019) showed that explanations may change simply due to applying a global mean shift in data (and features). To achieve a more realistic evaluation, we experiment in various training settings that can change explanations Dombrowski et al. (2022). We vary the model architectures that may learn different features or their regularization Ali et al. (2023) that may influence what features the models rely on. We also select datasets from diverse domains that can be large, multivariate, and multi-class and show that saliency methods behave differently depending on the dataset. We choose classification problems from the UCR repository and a more complex segmentation dataset. Our study aggregates a total of 729 experiments.

This section is divided into three parts. First, we discuss the metrics for the classification task (faithfulness, sensitivity, stability, robustness, sanity). Next, we investigate the influence of regularized model training on the faithfulness variants TS and TI

and explain their differences. Finally, we discuss the new localization metric for the segmentation task. The source code to reproduce our experiments is available at <https://github.com/crispchris/saliency>.

4.1 Experimental Setup

We evaluate nine visual interpretation methods: Gradient (Simonyan et al., 2014), Integrated Gradient (Sundararajan et al., 2017), SmoothGrad (Smilkov et al., 2017), Guided Backpropagation (Springenberg et al., 2015), GradCAM (Selvaraju et al., 2017), Guided-GradCAM (Selvaraju et al., 2017), Layer-Wise Relevance Propagation (LRP) (Bach et al., 2015), LIME (Ribeiro et al., 2016), and Kernel SHAP (Lundberg and Lee, 2017). See Appendix B.2 for method-specific hyper-parameters.

For the classification tasks, we select the two commonly used model architectures: Fully Convolutional Network (FCN) (Long et al., 2015) and Temporal Convolutional Network (TCN) (Bai et al., 2018). Due to noisy or vanishing saliency in preliminary studies, we do not focus on simpler architectures such as Multilayer Perceptrons and LSTMs (Hochreiter and Schmidhuber, 1997). Our dataset selection follows related work (Fawaz et al., 2019b; Wang et al., 2017; Schlegel et al., 2019; Ates et al., 2021) that uses large, multivariate, multi-class datasets from diverse domains (GunPointAgeSpan, FordA, FordB, ElectricDevices, MelbournePedestrian, and NATOPS) from the UCR repository (Dau et al., 2018). We study faithfulness under the influence of dropout and ℓ_1 - and ℓ_2 -regularization separately with experiments focusing on the FCN and the datasets FordA, FordB, and NATOPS. For the segmentation task, we consider two models: U-time (Perslev et al., 2019) (derived for time series from U-Net (Ronneberger et al., 2015)), and a bi-LSTM (Schuster and Paliwal, 1997). We provide details on each architecture in Appendix B.3. We evaluate them on the tool tracking (Löffler et al., 2021) dataset, a complex multivariate, multi-class time series from a 9-D magneto-inertial sensor, and use data from an electric screwdriver.

4.2 Evaluation on Classification Task

This section discusses the six visual interpretation quality metrics for the classification task. Fig. 3 summarizes the scores for each metric over model architectures and datasets. Fig. 4 summarizes the scores for each metric over model architectures and methods.

Faithfulness. We evaluated both variants of faithfulness metrics and found significant differences. In general, methods can achieve higher scores in the Temporal Importance variant compared to the Temporal Sequence. This indicates that the visualization methods can pinpoint individual features faithfully but fail to capture dependencies on longer sequences accurately. We also observe a relatively low correlation between methods - the visualizations that performed best in TI, i.e., GradCAM and Guided GradCAM, achieve only comparatively low scores in TS.

TS assumes that features are clustered and sequential. We hypothesize that this assumption is not valid for many time series domains. In particular, TS shows deficient scores of low variance for the FordA and NATOPS datasets in Fig. 4, which indicates that this assumption is potentially violated. The multivariate NATOPS seems to exhibit diversely distributed features. For these reasons, we focus the following discussion on TI.

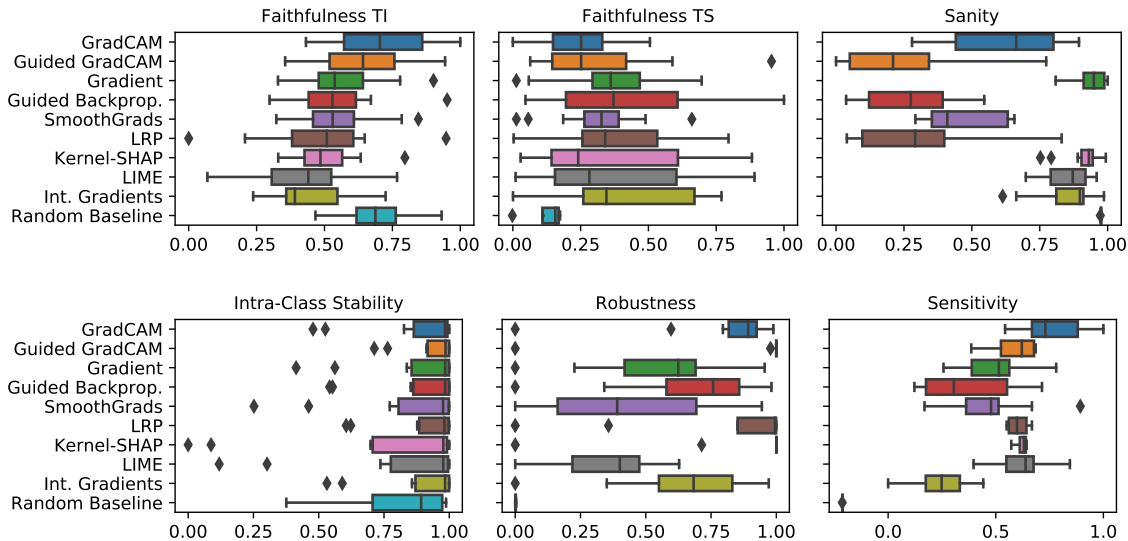


Figure 3: We aggregated results for TCN and FCN overall classification datasets {model architectures, datasets} without normalization (as we found that model architectures generally lead to similar scores).

The TI scores of GradCAM and Guided GradCAM are above average, and Integrated Gradients are below average. The more coarse GradCAM even slightly overtakes its Guided variant, likely due to GradCAM capturing the higher level features and Guided-GradCAM’s sample-level interpolation introducing a bias. Integrated Gradients may fail due to the bias introduced by its user-defined baseline. The other methods perform similarly on average. The dataset-centered view in Fig. 4 shows that the complex NATOPS dataset is the hardest to explain. This may be due to the potentially multi-dimensional features that are not perturbed.

Sanity. Across all datasets, we find that Gradient, Integrated Gradients, LIME, and Kernel-SHAP consistently achieve high sanity scores. In contrast, LRP, Guided GradCAM, and Guided Backpropagation often assign similar saliency even after randomizing network parameters. This replicates sanity results by Adebayo et al. (2018). Low sanity methods highlight features in the input that may also be randomly extracted but do not necessarily predict classes.

Intra-class Stability. This metric depends highly on the dataset, e.g., centered samples, as in GunPointAgeSpan. However, when accounting for variance introduced by the dataset (see Fig. 10b in Appendix C.2), SmoothGrads, LIME, and Kernel-SHAP show unstable saliency maps for the same classes. The location in the sample and the warped distance between samples using DTW differ. Guided GradCAM can produce highly stable saliency maps across all datasets, likely due to its lower resolution.

It is essential to notice that some datasets, e.g., FordA, do not necessarily have stable or similar features. However, many real datasets exhibit stable features across classes, as evidenced by considerably higher scores for the ElectricDevices, GunPointAgeSpan, MelbournePedestrian, and NATOPS datasets. We found that visual analysis of samples can

be a helpful indication for the inherent intra-class stability of datasets - datasets with high scores exhibit relatively straightforward temporal features in specific orders. In contrast, those with low scores generally showed less localized features.

Methods that introduce additional biases into the visualization calculations, like Integrated Gradients and Guided GradCAM, can produce highly stable saliency maps. LIME and Kernel-SHAP look at individual sample points independently and thus produce unstable saliency maps. We hypothesize that SmoothGrad’s addition of noise to sharpen the saliency maps can lead to an unintended side effect of over-sharpening and overly focusing the saliency map onto a single, sample-local feature that does not generalize to the rest of the dataset, which in turn leads to the low intra-class stability.

Robustness. Leaving aside the underlying model’s robustness, our evaluation of Gradient shows it is less robust, a finding that confirms Smilkov et al. (2017). Furthermore, LIME and, interestingly, SmoothGrads also show a low average robustness. The additive noise of SmoothGrads may compound and lead to diverging saliency maps. On the other hand, LRP, (Guided) GradCAM, and KernelSHAP show relatively robust saliency maps. Compared to purely gradient-based metrics, LRP and GradCAM use class activations, which might have a regularizing effect. Similarly, Kernel-SHAP can be considered a more constrained version of LIME. The saliency methods should capture the underlying model’s robustness and not produce saliency for divergent behavior due to introduced biases. The robustness metric’s weakness is its computational cost: on {TCN,ElectricDevices} it reaches its time-out of 12 days.

Sensitivity. GradCAM shows the highest sensitivity for classes - the saliency maps for the most and least likely classes differ vastly. On the other hand, Integrated Gradient and Guided Backpropagation produce similar saliency maps independent of a sample’s class. This holds across all datasets. A possible explanation is that methods that introduce additional biases into the visualization calculations might lead to less sensitive saliency maps. Integrated Gradients integrates from a user-defined baseline. Guided Backpropagation intentionally suppresses the negative part of the gradient signals to find more visually focused and intuitive interpretations. While these biases can improve the visual appeal of the saliency maps, our results suggest that they have a not negligible impact on saliency maps and should be avoided when sensitivity is a concern.

4.3 Influence of Datasets and Models

First, datasets heavily impact scores, see the outliers in Fig. 3. The plots of the categories over each dataset for all {model architectures, methods} in Fig. 4 emphasize this finding. The choice of visual interpretation method depends, for the most part, on the task. Still, after normalizing for dataset bias, the relative scores do not diverge significantly but confirm the initial scores. We report the relative scores in Fig. 10b in Appendix C.2.

Surprisingly, the model architecture (FCN or TCN) only contributes little to the scores, see Fig. 10c in Appendix C.2. The scores for FCN and TCN diverge slightly more for faithfulness TS and TI. This may be due to the higher capacity of the TCN, which learns more diverse features so that its TS score is lower and its TI score is higher. The FCN

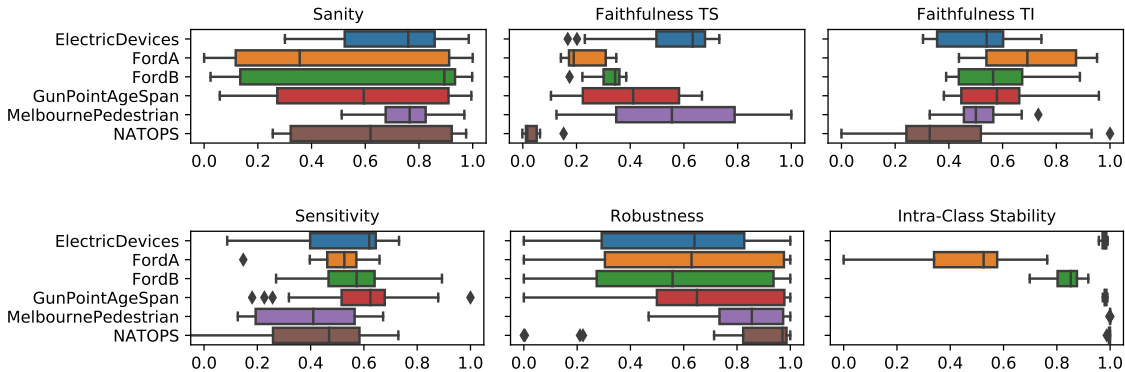


Figure 4: The plots show the influence of datasets on the scores when we aggregate for each dataset over {model architectures, methods}. Similarity metrics for saliency maps yield different results in different domains.

may learn fewer and less predictive features that are clustered more but are overall less predictive, resulting in higher TS scores and lower TI scores.

4.4 Influence of Regularization

Neural networks (among other parametric models) benefit from regularization techniques such as weight decay or dropout (Srivastava et al. (2014)). The positive effects can include increased accuracy and better generalization due to decreased overfitting of training data. However, we show that there are also unintended side effects of dropout, ℓ_1 , and ℓ_2 regularization on the faithfulness of saliency methods, for which we give recommendations. We focus this section on investigating faithfulness because other metrics only indirectly relate to accuracy and, thus, regularization.

Hypotheses. We hypothesize differences in faithfulness due to regularization effects. *Dropout regularization* can be understood as computing the average of several thinned networks (Srivastava et al., 2014). Regularized models rely less on individual features. Hence, models should score higher in Temporal Importance because of TI’s arbitrary choice of input features of the highest saliency and lower for Temporal Sequence, which is biased towards clusters of important features. Weight decay (Plaut et al., 1986), such as ℓ_1 or ℓ_2 regularization, should result in the opposite learning effect. An ℓ_1 loss term causes sparsity of the parameters and supports finding the smallest required feature set, which may also influence saliency Ali et al. (2023). Models may learn fewer features that are of higher importance (Krogh and Hertz, 1991). This should result in higher scores for TS. More specifically, ℓ_2 regularization optimizes models to learn more features of similar importance, thus equalizing the importance of learned features (Plaut et al., 1986). Hence, their saliency’s faithfulness should perform similarly to the TI and TS variants.

Accuracy. Fig. 5 shows how regularization impacts the accuracy of an FCN on FordA, FordB, and NATOPS in the top row of plots. We show the relative change from the non-regularized baseline, indicated by the hyper-parameter $\lambda = 0.0$, and average the results over two random seeds. Differences in accuracy vary between dropout, ℓ_1 , and ℓ_2 and also be-

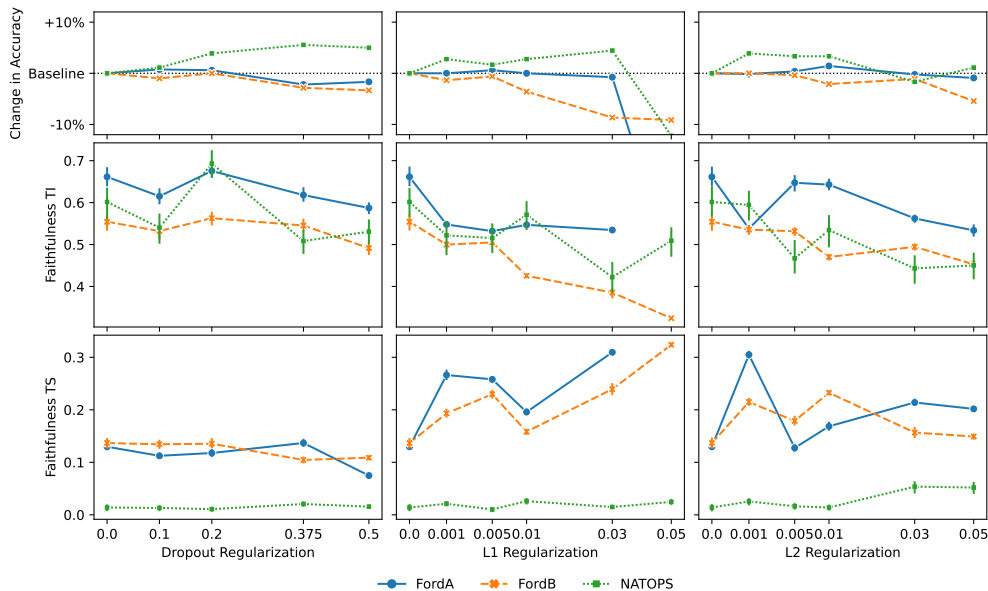


Figure 5: Accuracy (top), faithfulness TI (middle), and TS (bottom) scores for all visualizations across the FordA (blue), FordB (orange), and NATOPS (green) datasets.

tween datasets. The accuracy on the FordA dataset is relatively stable with regularization, except for an outlier at the large ℓ_1 reg. of $\lambda = 0.05$. In contrast, the accuracy declines on FordB, with a downward trend for increasing values of λ . Interestingly, the FCN benefits from regularization on the more complex NATOPS dataset. Dropout reliably improves accuracy, while the positive effect of weight decay is not as stable for larger λ of 0.05 (ℓ_1) and 0.03 (ℓ_2). The effect of a too large ℓ_1 weight decay is most detrimental; the model even fails to learn the two-class task FordA.

Absolute Faithfulness. We show the saliency methods’ aggregated Faithfulness TI and TS scores. Despite similar accuracy for the regularization schemes, faithfulness scores differ strongly. For TI, a small dropout regularization produces better saliency than ℓ_1 or ℓ_2 regularization across all datasets, even though the accuracy for models is close, e.g., models for FordA perform within 1%. Interestingly, the opposite holds for TS, where ℓ_2 regularization positively affects the FordA and FordB datasets. ℓ_1 regularization displays a similar effect on all datasets. This confirms our hypotheses that enforcing feature sparsity can affect faithfulness TI and TS differently. We observe outliers for dropout regularization with $\lambda = 0.2$, which markedly improved faithfulness scores across datasets. A meaningful faithfulness score could not be computed for ℓ_1 regularization with $\lambda = 0.05$ on FordA because the model did not exceed the performance of random guessing.

Accuracy and Faithfulness. Interestingly, we do not see that an increase in accuracy, e.g., for NATOPS or ℓ_2 with $\lambda = 0.01$, consistently correlates with an increase in a TI score. This may be due to the limited fraction of input values (we use 20%) that we perturb while calculating TI. However, a decrease in accuracy tends to come with worse TI. Additionally,

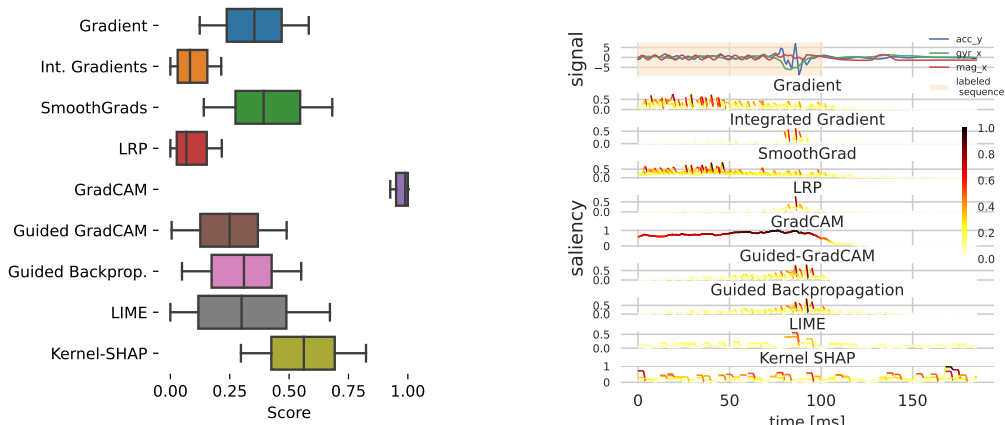
to less accurate models, there may be a second effect at play. The thinning of features due to weight decay leads to fewer learned features. Perturbing less predictive features naturally results in lower TI scores. The FCN’s concentration on fewer features with ℓ_1 regularization is especially apparent in the Ford datasets’ trends in TS. This faithfulness variant is biased towards clustered features and benefits from feature sparsity.

We conclude from these experiments that regularization is vital for accuracy and faithful saliency. Any faithfulness directly depends on the relationship between the accuracy of the models and saliency maps, even if it is not instantly apparent when using a fixed fraction of perturbation when calculating TI because regularization may increase or reduce feature sparsity in the model. Practitioners should choose a suitable regularization depending on the faithfulness variant. Similar test accuracy does not automatically imply similar faithfulness of saliency. This may be due to the numerical effects of weight decay and dropout on the networks’ parameters and feature learning.

4.5 Evaluation on Segmentation Task

This section presents the key findings from our evaluation when applying the localization metric on saliency maps generated from U-time (results for bi-LSTM are in Appendix C.1), trained for a segmentation task on the tool tracking dataset (Löffler et al., 2021). Fig. 6a shows each visualization method’s localization classical positional bias. Fig. 6b shows an exemplary saliency map for each method. Fig. 7 summarizes the statistics for the biases ”classic”, ”front”, ”middle” and ”back”.

At first glance, GradCAM produces saliency maps with top scores in the localization metric. Additionally, its saliency maps appear much smoother and continuous, with high relevance in the annotated segments. The high-fidelity saliency map of Guided GradCAM instead produces lower scores due to its more nuanced relevancy assignments. This difference



(a) U-time localization with a "classic" bias.

(b) U-time examples.

Figure 6: Results for the localization metric on the tool tracking dataset and with all methods on U-time. We show detailed values for the localization metric in (a) and examples of saliency maps in (b).

results from GradCAM’s coarser relevance, as its gradients do not flow to the input but stop at the last convolution layer. In contrast, LRP and Integrated Gradient produce lower scores. As Fig. 6b shows, the saliency maps highlight fewer relevant input features for the segmentation task but instead features within the labeled sub-sequence that may be important for classification.

Analyzing the scores in Fig. 7 shows that saliency maps are located more in the ”middle” of the annotated segments, compared to ”front” and ”back”. This is also visible in the example in Fig. 6b where the relevance values start decreasing below the threshold of 0.5 already before the end of the labeled segment at 100 ms. This points towards a biased labeling process with longer sub-sequences assigned to the classes than necessary and can help identify faulty labels. Furthermore, the high variance of most results (except for GradCAM) shows that saliency maps for time series segmentation are noisy. This is especially true for Kernel SHAP, where relevance is apparently assigned randomly.

GradCAM assigns saliency nearly perfectly to the labeled segments, compared to the other methods in this study that only marginally align with the annotated segments in the input features. Their saliency maps are comparatively noisy. However, each method’s faithfulness must be considered before choosing a saliency method to trust for producing interpretations, locating faulty labels, or even spurious correlations. Interestingly, no method worked reliably on the bi-LSTM. We identify a lack of helpful visualization methods for LSTMs, as CAM variants (GradCAM, Guided GradCAM, and Guided Backprop) are not applicable, see Fig. 9 in Appendix C.1 for detailed results.

In summary, localization scores of saliency for faithful models provide helpful analysis of temporal biases and label inconsistencies and can support the detection of shortcut learning. It is a red flag if an otherwise faithful saliency method has a low overlap of the saliency map and the potentially faulty label, or spurious correlations may be present. If saliency maps lie well within the labeled sub-sequence, but the saliency itself is not faithful, the score may hint at a bias in the saliency method.

5. Recommendations

The quality of visualizations differs significantly between methods. No method passes the tests for all categories on all six datasets. This emphasizes the need to evaluate all metrics for every visual interpretation. We recommend using a summary as in Fig. 8 to judge visualizations on every category and propose the following guidelines for relative ranking. The absolute scores may be understood compared to a random baseline, similar to shuffled AUC (Borji et al., 2013).

Setup model training and regularization hyperparameters. As an initial step, we recommend selecting a suitable set of regularization methods and their hyperparameters to optimize the models, depending on the task at hand. Dropout, ℓ_1 - or ℓ_1 -regularization may have a significant effect on the model’s inductive bias and thus also on faithfulness.

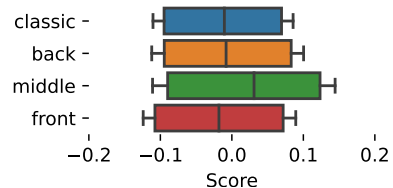


Figure 7: Localization biases for visualization methods on the tool tracking dataset.

This also depends on the datasets’ feature distribution. Note that the right regularization can meaningfully improve the model interpretability, and we suggest changing parameters if objective metrics indicate a low trust in visualizations.

First: Ensure Faithfulness and Sanity. The general purpose of interpretability methods is to provide insights into model behavior. We propose to use the faithfulness and sanity scores to ascertain that a saliency map represents the model behavior. Faithfulness ensures that the saliency matches the model’s predictive features. Note that, depending on the prevalence of temporal correlations and sequential features in a dataset, an expert should choose between TS (when sequential features are essential) and TI (when this is not the case). When in doubt, we propose to use TI.

Sanity checks confirm that saliency maps are sensitive to model parameters. This is important to avoid finding highly salient features, such as edges in images (Adebayo et al., 2018) while being insensitive to model parameters. We avoid saliency maps with low scores in either metric, as they do not reflect the model behavior. See Fig. 8 for an example: Gradient, Integrated Gradients and LIME achieve the three highest-ranked scores. However, *random saliency maps* (second to the last column) are dissimilar (hence they also show high sanity scores), and their relatively high TI score of 0.57 hints that the faithfulness of the other methods is not entirely reliable and additional tests are required. Guided Backprop, Guided GradCAM, and LRP fail the sanity check, while Kernel-SHAP performs poorly in faithfulness.

Second: Check Sensitivity and Robustness. Once faithfulness and sanity are established, we propose to look at the sensitivity and robustness of the generated saliency maps. A low inter-class sensitivity can indicate that the saliency maps only focus on the predicted class and underestimate the importance of features that do not belong to this class. A low robustness score suggests that the visualization method is susceptible to adversarial

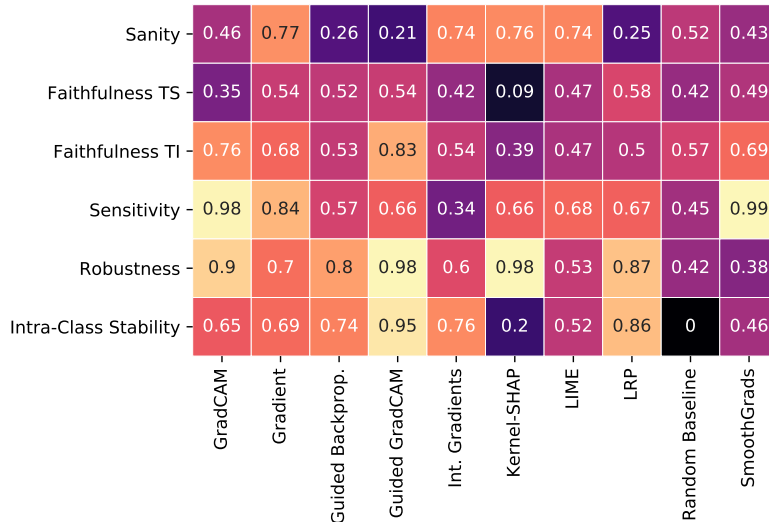


Figure 8: Scores as a heat map for TCN on FordB. Columns with high relative scores (bright squares) indicate good visualizations. Dark squares show the shortcomings.

examples and small perturbations in the input. Given that the model predictions are robust (Zhang et al., 2019), and the saliency is faithful, low robustness implies that the saliency method cannot be trusted and may even be manipulated (Dombrowski et al., 2019). We recommend relying less on visual interpretations for non-robust models, especially if they have low faithfulness. According to Fig. 8, we keep Gradient and LIME but disregard Integrated Gradients due to its lower sensitivity.

Detailed Analysis: Analyze Intra-class Stability and Localization. Intra-class stability measures how much saliency maps for one class agree between different samples. Like other Pointing Game-like metrics, the localization metric measures semantic precision based on annotations. They allow experts to choose and analyze saliency methods that are more intuitive and understandable. Note that it is crucial to ensure the faithfulness of a method before relying on this metric. If the method is not faithful, stable and localized visualizations are visually pleasing but do not reflect model behavior. This can hide issues like spurious correlations (Arjovsky et al., 2019) or the shortcut learning problem (Geirhos et al., 2020) behind a higher score.

6. Conclusion

We propose an evaluation scheme for visual interpretations of time series data. We provide extensive empirical results for different visualizations, models, datasets, and regularization methods across time series classification and segmentation. We recommend six orthogonal metrics that provide a disentangled evaluation of essential characteristics of visual interpretations. All these metrics should be evaluated for every visual interpretation to prevent relying on interesting but spurious results. We also show how each perspective evaluates different strengths and weaknesses of visualization methods and give recommendations on their use. The main findings are:

- No individual visualization method achieves high scores on all evaluation methods. For practitioners, we thus recommend focusing on faithfulness (TI) and sanity first.
- The strong impact of datasets on the saliency methods was consistent across all evaluation perspectives. This indicates that the interpretability of the underlying model is similarly dependent on the learned distribution as its predictive accuracy.
- Similarly, visual interpretation methods may introduce an additional bias into the visualization calculations. We show that this can lead to highly stable saliency maps.
- Regularization during training had a large but inconsistent influence on faithfulness. High regularization tends to decrease TI but increases the TS variant.
- Model architecture of convolutional networks alone had a relatively low impact on evaluation scores for visualization methods, compared to MLP or LSTM, which were noisy or suffered from vanishing saliency.
- Our novel localization metric for segmentation analyzes if saliency is assigned correctly to local features and helps to evaluate label ranges. GradCAM displays an outstanding localization of features, surpassing other methods.

Overall, our work demonstrates how the explanations of state-of-the-art visualization methods differ wildly. Experts can distinguish between plausible but wrong saliency maps using faithfulness and sanity scores. Since visualization methods are used to explain neural networks to human experts, more quality measures are necessary. Explanations must be sensitive for classes, robust (if the model is robust), and stable (if the model operation is consistent) while staying faithful to the model behavior. We combine these requirements into a straightforward framework that can be used to assess visual interpretations of time series data for arbitrary neural networks.

Future work investigates the relatively high scores of the random baseline in the two main metrics, sanity and faithfulness. Furthermore, our regularization study shows results that align with previous work Dombrowski et al. (2022). Model training should be optimized for more reliable interpretability so that they behave more intuitively without sacrificing predictive performance. Finally, the localization metric may be adapted to detect spurious correlations in time series problems.

REPRODUCIBILITY

This paper includes supplemental materials to improve reproducibility. Most importantly, we publish the code for model training and dataset loaders to generate visual interpretations of all evaluation metrics. Furthermore, all datasets are publicly available.

Acknowledgments

This work was supported by the IFI program of the German Academic Exchange Service (DAAD), the Bavarian Ministry of Economic Affairs, Infrastructure, Energy and Technology as part of the Bavarian project Leistungszentrum Elektroniksysteme (LZE) and through the Center for Analytics-Data-Applications (ADA-Center) within the framework of "BAYERN DIGITAL II".

Appendix A.

A. Localization Metric Positional Biases

This section explains our localization metric’s ”existence” and ”overlap” terms. Note again the recall score as

$$S_{\text{recall}}(Y_{\text{sub}}, Y') = \alpha \cdot \text{existence}(Y_{\text{sub}}, Y') + (1 - \alpha) \cdot \text{overlap}(Y_{\text{sub}}, Y'), \quad (10)$$

The ”existence” and ”overlap” terms are defined by Tatbul et al. (2018) as follows. First, existence is defined as a correct prediction of one sample point at index j of the correct class within the labeled region:

$$\text{existence}(Y_{\text{sub}}, Y') = \begin{cases} 1, & \text{if } \sum_{j=1}^{|Y'|} |Y_{\text{sub}} \cap Y'_j| \geq 1 \\ 0, & \text{otherwise} \end{cases} \quad (11)$$

The overlap determines the finer properties cardinality $\gamma()$, size $\omega()$ and position $\delta()$.

$$\text{overlap}(Y_{\text{sub}}, Y') = \text{cardinality}(Y_{\text{sub}}, Y') \cdot \sum_{j=1}^T \omega(Y_{\text{sub}}, Y_{\text{sub}} \cap Y'_j, \delta) \quad (12)$$

$$\text{cardinality}(Y_{\text{sub}}, Y') = \begin{cases} 1, & \text{if } Y_{\text{sub}} \text{ overlaps with at most one } Y'_j \in Y' \\ \gamma(Y_{\text{sub}}, Y'), & \text{otherwise} \end{cases} \quad (13)$$

The term α ($0 \leq \alpha \leq 1$) weights existence and the following qualitative overlap measures. The three user-defined functions return values of $0 \leq \gamma() \leq 1$, $0 \leq \omega() \leq 1$ and $\delta() \geq 1$. The cardinality $\gamma()$ function weighs the prediction of a continuous range Y' covering the whole labeled range Y_{sub} versus interrupted ranges in a fragmented manner. The overall size $\omega()$ of the agreement of predicted and label ranges depends on the positional bias $\delta()$ and can favor ”front”, ”middle”, or ”back”. Practically, for some applications, early detection is preferable to late detection. For the four functions, we selected α is equal to 0, γ is equal to 1. ω depends on the position bias δ and for δ we have three variants, ”front”, ”middle” or ”back”, proposed by Tatbul et al. (2018).

B. Experimental Setup

We describe each visual interpretation method shortly in Sec. B.1, then the hyperparameters for each visual interpretation method in Sec. B.2 and for the optimizer and networks in Sec. B.3.

B.1 Categorization of Methods

This Section provides a short introduction to the methods that we use in our experiments.

Gradient-based methods. Gradient (Simonyan et al., 2014) computes class c ’s saliency map M^c using the derivative of the class score P^c of model with respect to the input sample x , as $M^c(x) = \frac{\partial P^c}{\partial x}$. However, Gradient suffers from the *saturation problem* (a feature may have global importance, but its local derivative is small (Smilkov et al., 2017)), local

sensitivity, and noisy saliency maps (due to (sharp) local variations in the gradients (Smilkov et al., 2017)). Follow-up work smooths the gradients to reduce noise (Smilkov et al., 2017), applies special propagation rules instead of propagating a gradient (Arras et al., 2017), or propagates only up to a specific intermediate layer (Selvaraju et al., 2017).

Perturbation-based methods. Ribeiro et al. (2016) proposed Local Interpretable Model-Agnostic Explanations (LIME) that fit a local surrogate model (e.g., a linear regression) as an explanation and use this surrogate to calculate relevance. Kernel SHAP (Lundberg and Lee, 2017) builds on LIME but calculates Shapley values that measure the contribution of individual features to the input more accurately.

B.2 Visualization Methods Hyper Parameters

We set the hyperparameters for each visual interpretation method according to their recommendations from the literature. We provide the reasoning behind the selected parameters in the following paragraphs.

Gradient computes the derivative of the target class score for the input sample and returns the saliency map of the input sample at the end. Integrated Gradient uses the linear path method to compute Gradient along the path from a baseline x' . We use a zero vector for the baseline. As suggested by Smilkov et al. (2017), the number of steps for the path should be selected between 20 and 300. Hence, we use steps $N = 60$, meaning that it takes 60 steps from baseline x' to the original input sample x , according to $x = x' + \frac{(x-x')}{N} \cdot n$, n is the current step.

SmoothGrad also computes the input sample’s derivative of the target class score. However, it adds Gaussian noise $\mathcal{N}(0, \sigma^2)$ to the input sample multiple times and computes the gradients from the perturbed samples ($x + \mathcal{N}(0, \sigma^2)$). The number of iterations of adding noise is chosen $N = 60$ and the standard deviation of Gaussian noise is chosen $\sigma = 0.2$.

For LRP, we select the ϵ -propagation rule for every DL model with $\epsilon = 1e - 9$. Due to the residual block in the TCN model, the propagated relevances should be added together ($R = R_1 + R_2$).

GradCAM and Guided-GradCAM are designed for models with convolutional layers, i.e., FCN, TCN, and U-time. GradCAM focuses on the last convolutional layer, which produces feature maps, whose shapes are usually smaller than the shape of input samples. Therefore, we use interpolation to up-sample the saliency maps from the last convolution layer to match their shape to the shape of the input samples, which allows us to visualize them in the input space. Because of ReLU functions, GradCAM returns only positive relevances.

For LIME, we use the cosine distance function as the kernel function with width $w = 5.0$ to weight the perturbed samples and perform 1000 iterations. For the perturbation, we consider that neighbors along the time dimension should have similar relevance to reducing the computational time, so we set the number of features along the time dimension 50 for GunPointAgeSpan. This means that saliency maps for samples with length 150 in GunPointAgeSpan have the same relevance for every 3 neighbors, and saliency maps for dense labeling samples in tool tracking have the same relevance for every 4 neighbors.

We use 1000 iterations for Kernel SHAP and set the number of features along the time dimension to 50. Furthermore, the sampling of feature perturbation in Kernel SHAP is

based on the distribution $p(f) = \frac{(F-1)}{(f \cdot (F-f))}$, where f is the number of selected features and F is the total number of features in interpretation space.

B.3 Network Architectures

We use the Adam optimizer with a learning rate of 0.002. We train every dataset for 600 epochs (with early stopping after 80 epochs). We use a Cross-Entropy loss for time series classification and a Generalized Dice loss with a Cross-Entropy function for time series segmentation.

For the time series segmentation task on the tool tracking dataset, we report an accuracy of 83% for U-time and 85% for the bi-LSTM. Table 1 shows the classification results for FCN and TCN with all classification datasets.

datasets	model architectures	
	FCN	TCN
GunPointAgeSpan	88.38 \pm 2.44	95.91 \pm 2.27
FordA	89.43 \pm 0.31	91.42 \pm 0.35
FordB	75.47 \pm 1.71	79.38 \pm 1.31
MelbournePedestrian	90.94 \pm 0.98	88.39 \pm 5.23
NATOPS	95.79 \pm 1.56	90.0 \pm 7.09
ElectricDevices	67.49 \pm 2.44	68.0 \pm 1.96

Table 1: The test accuracy in % of the classification task.

B.3.1 FULLY CONVOLUTION NETWORK

We use a slightly modified FCN, similar to Wang et al. (2017). Ours contains four convolution blocks with a convolutional layer, a batch normalization layer (Ioffe and Szegedy, 2015) and a ReLU layer in each block. The kernel shapes and numbers of filter for convolution layers are $\{7, 5, 3, 3\}$ and $\{16, 32, 32, 16\}$. Therefore, there are four convolutional layers. Each convolutional layer has a unit stride and no padding, which means the time sequence will be reduced continuously by the blocks. The final convolution block, which is behind the four convolution blocks, does not have a ReLU layer and contains a 1x1 convolutional layer. The 1x1 convolutional layer serves as a projection layer. It can reduce the channel size of feature maps and keep their salient features. Finally, we apply Global Max Pooling on the features maps before the softmax operation.

B.3.2 TEMPORAL CONVOLUTION NETWORK

We use a global pooling layer for the prediction for the TCN, which was first proposed by (Bai et al., 2018). In our architecture, TCN has the convolution filters $\{16, 32, 32, 32\}$, and kernel shapes for convolution layers $\{7, 5, 5, 5\}$ in four residual blocks. Therefore, the total number of layers is 8.

B.3.3 BIDIRECTIONAL LONG SHORT-TERM MEMORY

We use a standard, single-layer bi-LSTM to predict dense labels for the segmentation task, as implemented in PyTorch, with 512 hidden units. There is a dense layer behind the LSTM model to fit the hidden units 512 to the number of classes. Also, the dropout rate is set to 0.2 to prevent overfitting.

B.3.4 U-TIME

We use the U-time (Perslev et al., 2019) architecture with the following configuration. Each convolution block has two dilated convolution layers with dilation 3, followed by a ReLU layer, a batch normalization layer, and a Max-Pooling layer at the end. The number of filters for convolution layers in four convolution blocks is $\{16, 32, 64, 128\}$ and the pooling window sizes are all 2. Two additional convolutions with filter numbers $\{256, 256\}$ follow after four convolution blocks. In each transposed convolution block, a nearest-neighbor up-sampling (Odena et al., 2016) of its input is implemented, followed by a dilated convolution layer with dilation 3, a ReLU layer, and a batch normalization layer. The number of filters for convolution layers in four transposed convolution blocks is in the reverse order of the encoder $\{128, 64, 32, 16\}$. The kernel size of convolution layers in both encoder and decoder is 7.

C. Additional results

We report additional results to supplement our discussion for a bi-LSTM architecture on the segmentation task in Sec. C.1 and for the classification task in Sec. C.2.

C.1 Evaluation on Segmentation Task: bi-LSTM

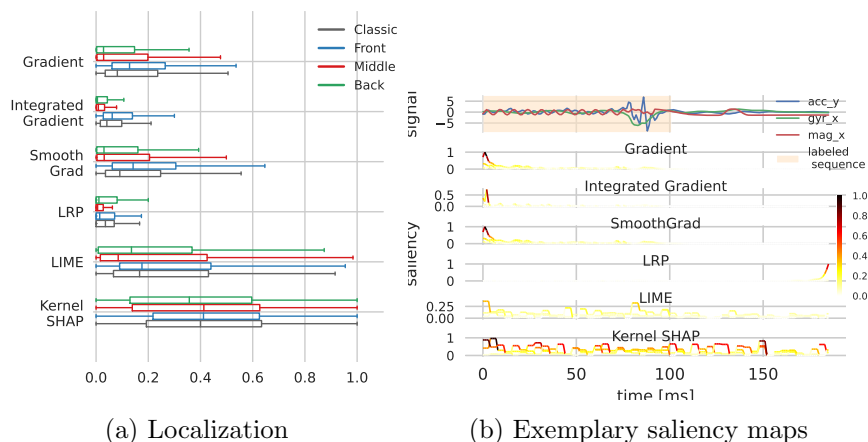


Figure 9: We show the localization metric results for all methods on the tool tracking dataset and with the bi-LSTM model. (a) shows the results for the localization metric. (b) shows exemplary saliency maps.

The results for bi-LSTM on the segmentation task for tool tracking in Fig. 9 show that none of the visual interpretation methods compatible with the model’s architecture produce satisfactory saliency maps.

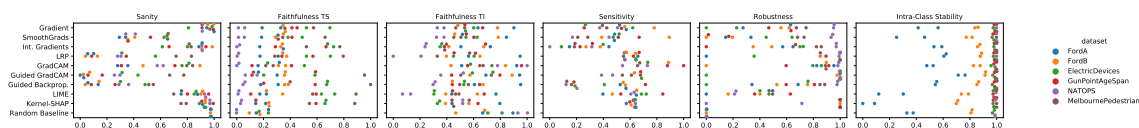
C.2 Classification Task

We show the variability of each visualization method for each dataset and metric category for the TCN in Fig. 10a. Notably, some datasets are more problematic for the methods, especially for faithfulness and intra-class stability, than others. We also show that the model has only a small influence. For this result, we aggregate all datasets and visualization methods separately for FCN and TCN in Fig. 10c.

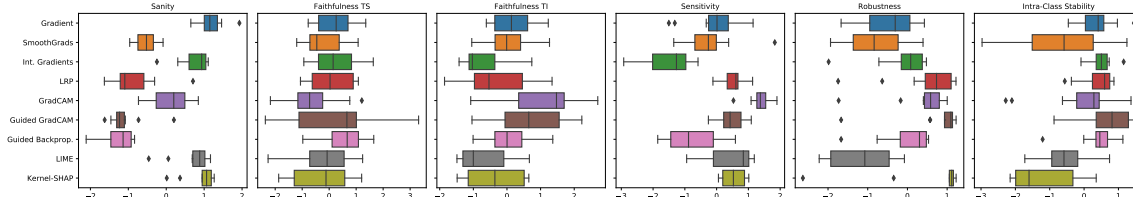
To compare methods independent of datasets, we control for their bias by normalizing the scores of all methods for each {category, dataset} so that their mean is 0 and variance is 1. With this, we can correctly assess the ”relative” performance of the visual interpretation methods across different datasets. The plot in Fig. 10b shows these relative (or marginal) scores that a method can achieve compared to other methods on the same datasets.

We prove the orthogonality of metrics in Figure 11. No combination of our metric scores shows a high correlation. This indicates that each metric measures a quality independent of all other metrics.

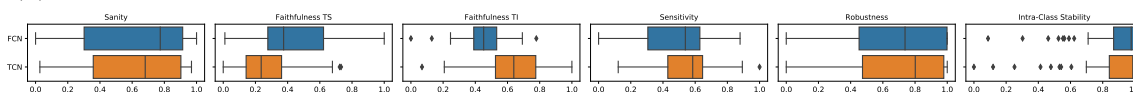
We show examples of the saliency of the TCN architecture on the FordB dataset for the visual interpretation methods for class 0 in Figure 12 and class 1 in Figure 13. We argue that our framework should guide the choice of a suitable method to generate saliency maps.



(a) Separated datasets.



(b) Relative scores that a method can achieve compared to other methods on the same datasets.



(c) Results for different model architectures, aggregated across datasets and visual interpretability methods. Model architecture has a comparatively small influence on the performance, which speaks to their generalization capabilities.

Figure 10: (a) shows scores separately over all {model, method } combinations. (b) removes the datasets’ bias to assess the performance of individual visual interpretability metrics independent from datasets. (c) shows results for different model architectures aggregated across datasets and visual interpretability methods. Model architecture has a comparatively small influence on the performance, which speaks to their generalization capabilities.

References

- J. Adebayo, J. Gilmer, M. Muelly, I. Goodfellow, M. Hardt, and B. Kim. Sanity checks for saliency maps. In *Advances in Neural Information Processing Systems*, pages 9505–9515, Montreal, Canada, 2018. Curran Associates, Inc.
- C. Agarwal, N. Johnson, M. Pawelczyk, S. Krishna, E. Saxena, M. Zitnik, and H. Lakkaraju. Rethinking Stability for Attribution-based Explanations. *arXiv preprint arXiv:2203.06877*, 2022.
- S. Ali, T. Abuhmed, S. El-Sappagh, K. Muhammad, J. M. Alonso-Moral, R. Confalonieri, R. Guidotti, J. Del Ser, N. Díaz-Rodríguez, and F. Herrera. Explainable Artificial Intelligence (XAI): What we know and what is left to attain Trustworthy Artificial Intelligence. *Information Fusion*, 99:101805, 2023. ISSN 15662535. doi: <https://doi.org/10.1016/j.inffus.2023.101805>.
- D. Alvarez-Melis and T. S. Jaakkola. On the robustness of interpretability methods. In *Proceedings of the 2018 ICML Workshop in Human Interpretability in Machine Learning*, Stockholm, Sweden, 2018.
- C. J. Anders, L. Weber, D. Neumann, W. Samek, K.-R. Müller, and S. Lapschkin. Finding and removing Clever Hans: Using explanation methods to debug and im-

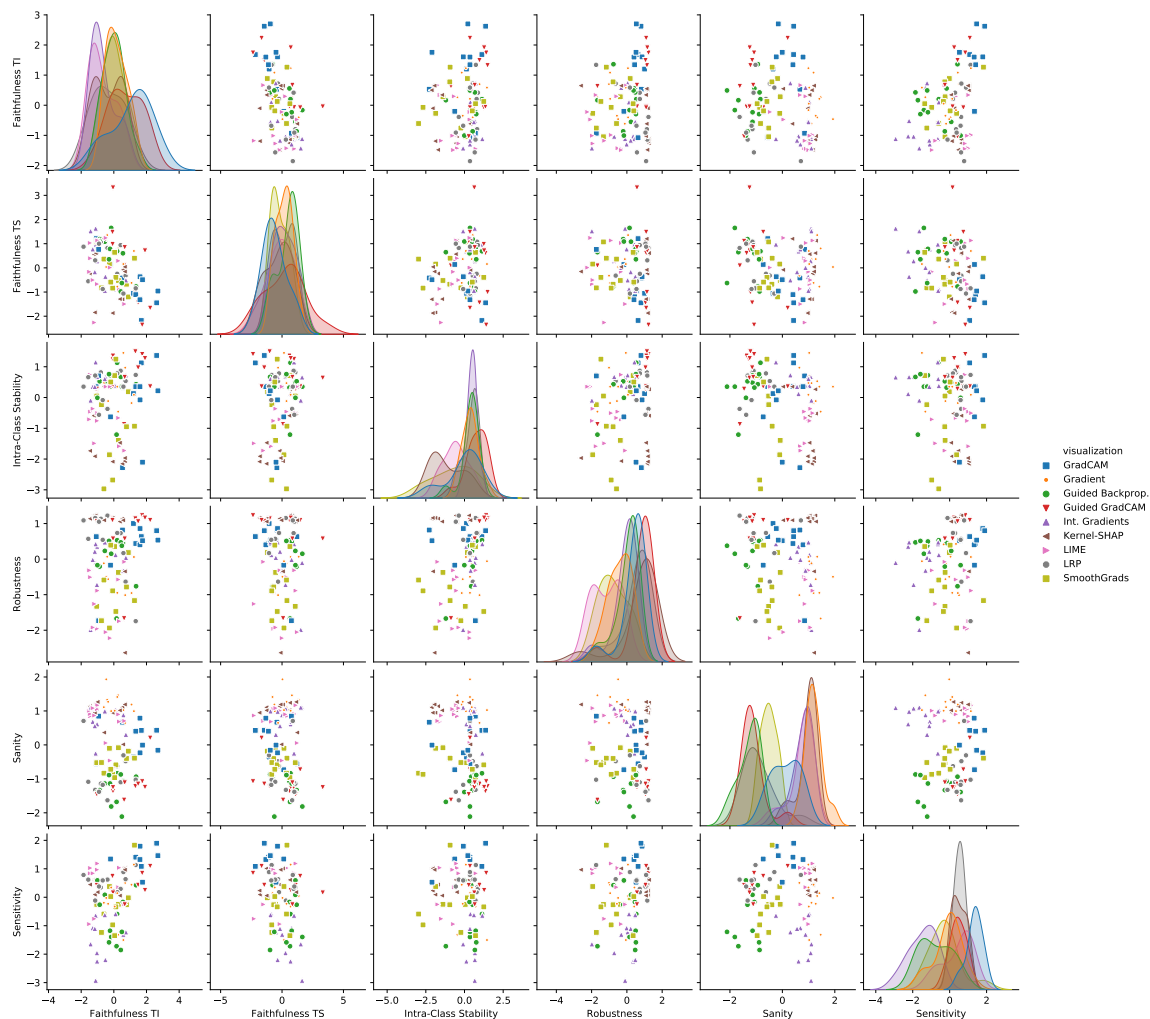


Figure 11: Pairplots of the correlations of metric scores with each other. No combination of metrics has a meaningful correlation with each other, proving that they provide independently helpful signals. This analysis is based on scores normalized for dataset bias, but the results also hold when this normalization is not done.

prove deep models. *Information Fusion*, 77:261–295, 2022. ISSN 1566-2535. doi: 10.1016/j.inffus.2021.07.015. URL <https://www.sciencedirect.com/science/article/pii/S1566253521001573>.

M. Arjovsky, L. Bottou, I. Gulrajani, and D. Lopez-Paz. Invariant risk minimization. *arXiv preprint arXiv:1907.02893*, 2019.

L. Arras, G. Montavon, K.-R. Müller, and W. Samek. Explaining recurrent neural network predictions in sentiment analysis. In *Proceedings of the 8th Workshop on Computational Approaches to Subjectivity, Sentiment and Social Media Analysis*, pages 159–168, Copenhagen, Denmark, Sept. 2017.

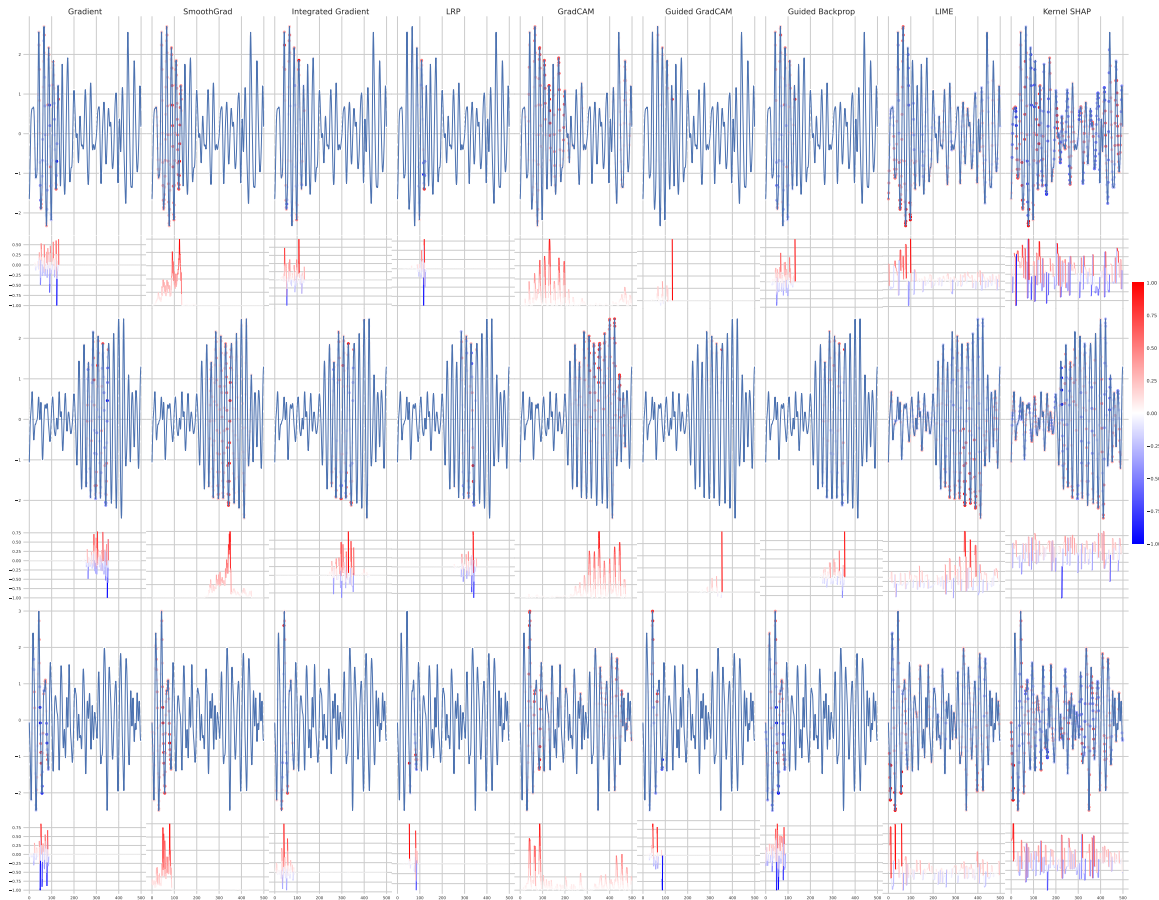


Figure 12: Examples of saliency maps for the TCN architecture on the FordB dataset for class 0.

A. B. Arrieta, N. Díaz-Rodríguez, J. Del Ser, A. Bennetot, S. Tabik, A. Barbado, S. García, S. Gil-López, D. Molina, R. Benjamins, et al. Explainable artificial intelligence (xai): Concepts, taxonomies, opportunities and challenges toward responsible ai. *Information Fusion*, 58:82–115, 2020.

E. Ates, B. Aksar, V. J. Leung, and A. K. Coskun. Counterfactual explanations for multivariate time series. In *2021 International Conference on Applied Artificial Intelligence (ICAPAI)*, pages 1–8, Halden, Norway, May 2021.

S. Bach, A. Binder, G. Montavon, F. Klauschen, K.-R. Müller, and W. Samek. On pixel-wise explanations for non-linear classifier decisions by layer-wise relevance propagation. *PLOS ONE*, 10(7):1–46, 07 2015. doi: 10.1371/journal.pone.0130140.

D. Baehrens, T. Schroeter, S. Harmeling, M. Kawanabe, K. Hansen, and K.-R. Müller. How to Explain Individual Classification Decisions. *Journal of Machine Learning Research*, 11:1803–1831, 2010.

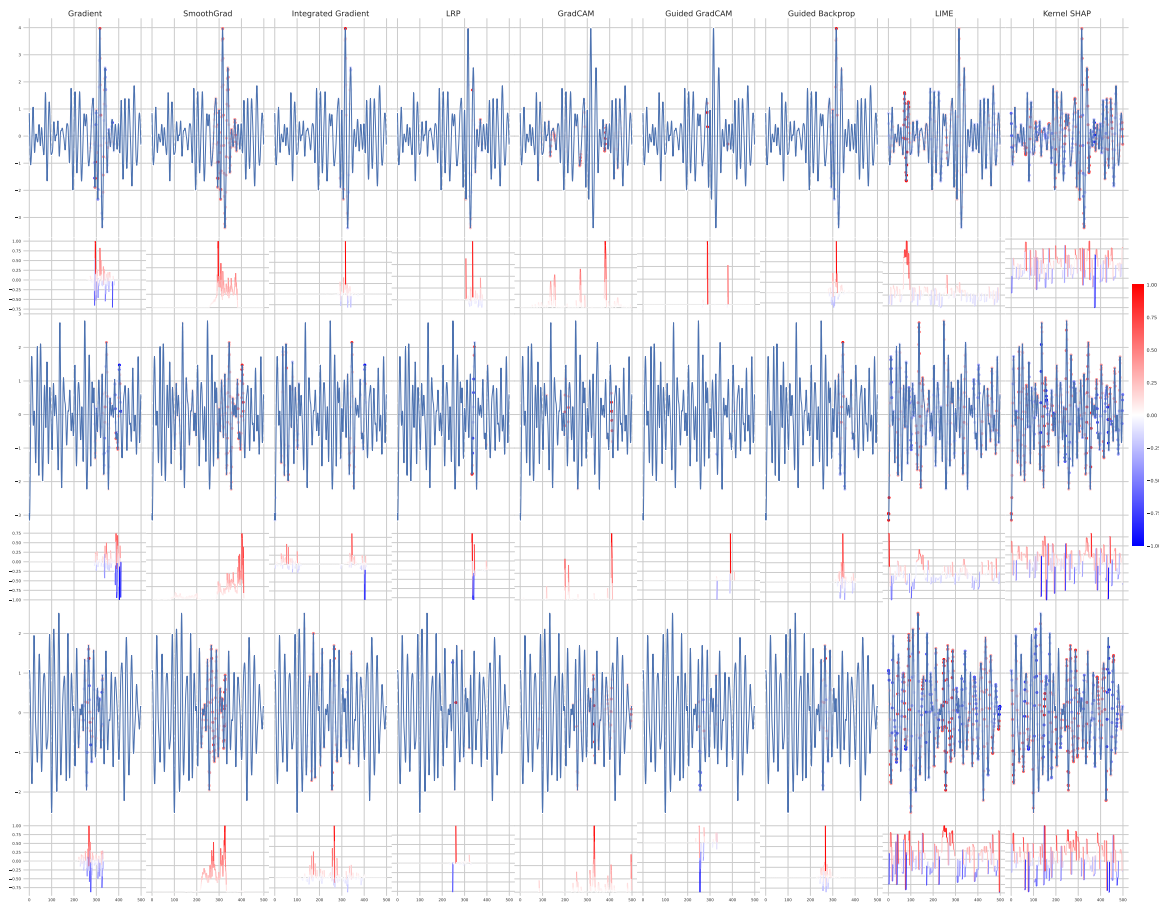


Figure 13: Examples of saliency maps for the TCN architecture on the FordB dataset for class 1.

- S. Bai, J. Z. Kolter, and V. Koltun. An empirical evaluation of generic convolutional and recurrent networks for sequence modeling. *arXiv preprint arXiv:1803.01271*, 2018.
- F. Berkenkamp, M. Turchetta, A. P. Schoellig, and A. Krause. Safe model-based reinforcement learning with stability guarantees. In *Proceedings of the 31st International Conference on Neural Information Processing Systems*, page 908–919, Long Beach, CA, 2017.
- A. Borji, H. R. Tavakoli, D. N. Sihite, and L. Itti. Analysis of scores, datasets, and models in visual saliency prediction. In *Proceedings of the IEEE International Conference on Computer Vision (ICCV)*, Sydney, Australia, December 2013.
- D. V. Carvalho, E. M. Pereira, and J. S. Cardoso. Machine learning interpretability: A survey on methods and metrics. *Electronics*, 8(8):832, Jul 2019. ISSN 2079-9292.
- I. C. Covert, S. Lundberg, and S.-I. Lee. Explaining by Removing: A Unified Framework for Model Explanation. *Journal of Machine Learning Research*, 22:90, 2021.

- H. Dau, A. Bagnall, K. Kamgar, M. Yeh, Y. Zhu, S. Gharghabi, and C. Ratanamahatana. The UCR time series archive. *ArXiv e-prints*, arXiv:1810.07758, 2018.
- A.-K. Dombrowski, M. Alber, C. Anders, M. Ackermann, K.-R. Müller, and P. Kessel. Explanations can be manipulated and geometry is to blame. In H. Wallach, H. Larochelle, A. Beygelzimer, F. d'Alché-Buc, E. Fox, and R. Garnett, editors, *Advances in Neural Information Processing Systems*, volume 32, Vancouver, Canada, 2019. Curran Associates, Inc.
- A.-K. Dombrowski, C. J. Anders, K.-R. Müller, and P. Kessel. Towards robust explanations for deep neural networks. *Pattern Recognition*, 121:108194, 2022. ISSN 00313203. doi: 10.1016/j.patcog.2021.108194. URL <https://linkinghub.elsevier.com/retrieve/pii/S0031320321003769>.
- E. Dorschky, M. Nitschke, C. Martindale, A. J. van den Bogert, A. Koelewijn, and B. Eskofier. CNN-Based Estimation of Sagittal Plane Walking and Running Biomechanics From Measured and Simulated Inertial Sensor Data. *Frontiers in Bioengineering and Biotechnology*, 8:1–14, 2020.
- F. Doshi-Velez and B. Kim. Towards a rigorous science of interpretable machine learning. *arXiv preprint arXiv:1702.08608*, 2017.
- H. I. Fawaz, G. Forestier, J. Weber, L. Idoumghar, and P.-A. Muller. Accurate and interpretable evaluation of surgical skills from kinematic data using fully convolutional neural networks. *International Journal of Computer Assisted Radiology and Surgery*, 14:1611 – 1617, 2019a.
- I. H. Fawaz, G. Forestier, J. Weber, L. Idoumghar, and P.-A. Muller. Deep learning for time series classification: a review. *Data Mining and Knowledge Discovery*, 33, 07 2019b.
- T. Fel and D. Vigouroux. Representativity and consistency measures for deep neural network explanations. *arXiv preprint arXiv:2009.04521*, 2020.
- T. Fel, D. Vigouroux, R. Cadene, and T. Serre. How Good is your Explanation? Algorithmic Stability Measures to Assess the Quality of Explanations for Deep Neural Networks. In *2022 IEEE/CVF Winter Conference on Applications of Computer Vision (WACV)*, pages 1565–1575, Waikoloa, HI, USA, 2022. IEEE. ISBN 978-1-66540-915-5. doi: 10.1109/WACV51458.2022.00163. URL <https://ieeexplore.ieee.org/document/9706798/>.
- R. Geirhos, J.-H. Jacobsen, C. Michaelis, R. Zemel, W. Brendel, M. Bethge, and F. A. Wichmann. Shortcut learning in deep neural networks. *Nature Machine Intelligence*, 2(11):665–673, 2020.
- B. Goodman and S. Flaxman. European union regulations on algorithmic decision-making and a “right to explanation”. *AI magazine*, 38(3):50–57, 2017.
- J. Han, M. Kamber, and J. Pei. 2 - getting to know your data. In *Data Mining (Third Edition)*, The Morgan Kaufmann Series in Data Management Systems, pages 39–82. Boston, 2012.

- A. Hedström, L. Weber, D. Krakowczyk, D. Bareeva, F. Motzkus, W. Samek, S. Lapuschkin, and M. M. M. Höhne. Quantus: An explainable ai toolkit for responsible evaluation of neural network explanations and beyond. *Journal of Machine Learning Research*, 24(34): 1–11, 2023. URL <http://jmlr.org/papers/v24/22-0142.html>.
- S. Hochreiter and J. Schmidhuber. Long short-term memory. *Neural Computation*, 9(8): 1735–1780, 1997.
- F. Horst, S. Lapuschkin, W. Samek, K.-R. Müller, and W. I. Schöllhorn. Explaining the unique nature of individual gait patterns with deep learning. *Scientific Reports*, 9(1): 2391, 2019. ISSN 2045-2322. doi: 10.1038/s41598-019-38748-8. URL <https://www.nature.com/articles/s41598-019-38748-8>.
- S. Ioffe and C. Szegedy. Batch normalization: Accelerating deep network training by reducing internal covariate shift. In *Proc. of the 32nd Intl. Conf. on Machine Learning*, page 448–456, Lille, France, 2015.
- A. A. Ismail, M. Gunady, H. Corrada Bravo, and S. Feizi. Benchmarking deep learning interpretability in time series predictions. In *Advances in Neural Information Processing Systems*, volume 33, pages 6441–6452, Vancouver, Canada, 2020. Curran Associates, Inc.
- Z. Jianming, L. Zhe, B. Jonathan, S. Xiaohui, and S. Stan. Top-down neural attention by excitation backprop. In *European Conference on Computer Vision(ECCV)*, Amsterdam, Netherlands, 2016.
- P.-J. Kindermans, S. Hooker, J. Adebayo, M. Alber, K. T. Schütt, S. Dähne, D. Erhan, and B. Kim. The (Un)reliability of Saliency Methods. In W. Samek, G. Montavon, A. Vedaldi, L. K. Hansen, and K.-R. Müller, editors, *Explainable AI: Interpreting, Explaining and Visualizing Deep Learning*, volume 11700, pages 267–280. Springer International Publishing, Cham, Switzerland, 2019. doi: 10.1007/978-3-030-28954-6_14.
- A. Krogh and J. Hertz. A simple weight decay can improve generalization. *Advances in neural information processing systems*, 4, 1991.
- S. Lapuschkin, S. Wäldchen, A. Binder, G. Montavon, W. Samek, and K.-R. Müller. Unmasking Clever Hans predictors and assessing what machines really learn. *Nature Communications*, 10(1):1096, 2019. ISSN 2041-1723. doi: 10.1038/s41467-019-08987-4. URL <http://www.nature.com/articles/s41467-019-08987-4>.
- S. Letzgus, P. Wagner, J. Lederer, W. Samek, K.-R. Müller, and G. Montavon. Toward Explainable Artificial Intelligence for Regression Models: A methodological perspective. *IEEE Signal Processing Magazine*, 39(4):40–58, 2022. ISSN 1053-5888, 1558-0792. doi: 10.1109/MSP.2022.3153277. URL <https://ieeexplore.ieee.org/document/9810062/>.
- X.-H. Li, Y. Shi, H. Li, W. Bai, C. C. Cao, and L. Chen. An experimental study of quantitative evaluations on saliency methods. In *Proceedings of the 27th ACM SIGKDD Conference on Knowledge Discovery & Data Mining*, pages 3200–3208, Singapore, 2021a.

- X.-H. Li, Y. Shi, H. Li, W. Bai, C. C. Cao, and L. Chen. An Experimental Study of Quantitative Evaluations on Saliency Methods. In *Proceedings of the 27th ACM SIGKDD Conference on Knowledge Discovery & Data Mining*, pages 3200–3208, Singapore, 2021b. Association for Computing Machinery. doi: 10.1145/3447548.3467148.
- C. Löffler, C. Nickel, C. Sobel, D. Dzibela, J. Braat, B. Gruhler, P. Woller, N. Witt, and C. Mutschler. Automated quality assurance for hand-held tools via embedded classification and automl. In *Machine Learning and Knowledge Discovery in Databases. Applied Data Science and Demo Track*, pages 532–535, Ghent, Belgium, 2021.
- J. Long, E. Shelhamer, and T. Darrell. Fully convolutional networks for semantic segmentation. In *Proceedings of the IEEE conference on computer vision and pattern recognition*, pages 3431–3440, Boston, MA, 2015.
- S. M. Lundberg and S.-I. Lee. A unified approach to interpreting model predictions. In *Advances in Neural Information Processing Systems*, volume 30, Long Beach, CA, 2017. Curran Associates, Inc.
- D. A. Melis and T. Jaakkola. Towards Robust Interpretability with Self-Explaining Neural Networks. In S. Bengio, H. Wallach, H. Larochelle, K. Grauman, N. Cesa-Bianchi, and R. Garnett, editors, *Advances in Neural Information Processing Systems*, volume 31, page 10, Montréal, Canada, 2018. Curran Associates, Inc.
- G. Montavon, W. Samek, and K.-R. Müller. Methods for interpreting and understanding deep neural networks. *Digital Signal Processing*, 73:1–15, 2018. ISSN 10512004. doi: 10.1016/j.dsp.2017.10.011. URL <https://linkinghub.elsevier.com/retrieve/pii/S1051200417302385>.
- A. Odena, V. Dumoulin, and C. Olah. Deconvolution and checkerboard artifacts. *Distill*, 1(10):e3, 2016.
- F. Oviedo, Z. Ren, S. Sun, C. Settens, Z. Liu, N. T. P. Hartono, S. Ramasamy, B. L. DeCost, S. I. Tian, G. Romano, et al. Fast and interpretable classification of small x-ray diffraction datasets using data augmentation and deep neural networks. *npj Computational Materials*, 5(1):1–9, 2019.
- M. Perslev, M. Jensen, S. Darkner, P. J. r. Jennum, and C. Igel. U-time: A fully convolutional network for time series segmentation applied to sleep staging. In *Advances in Neural Information Processing Systems 32*, pages 4415–4426, Vancouver, Canada, 2019. Curran Associates, Inc.
- D. C. Plaut, S. J. Nowlan, , and G. E. Hinton. Experiments on learning by back propagation. *Technical report, Carnegie-Mellon Univ., Pittsburgh, Pa. Dept. of Computer Science.*, 1986.
- S.-A. Rebuffi, R. Fong, X. Ji, and A. Vedaldi. There and back again: Revisiting backpropagation saliency methods. In *Conference on Computer Vision and Pattern Recognition (CVPR)*, Seattle, WA, 2020.

- M. T. Ribeiro, S. Singh, and C. Guestrin. “why should i trust you?”: Explaining the predictions of any classifier. In *Proceedings of the 22nd ACM SIGKDD International Conference on Knowledge Discovery and Data Mining*, page 1135–1144, San Francisco, CA, 2016.
- T. Rojat, R. Puget, D. Filliat, J. Del Ser, R. Gelin, and N. Díaz-Rodríguez. Explainable artificial intelligence (xai) on timeseries data: A survey. *arXiv preprint arXiv:2104.00950*, 2021.
- O. Ronneberger, P. Fischer, and T. Brox. U-net: Convolutional networks for biomedical image segmentation. In *Medical Image Computing and Computer-Assisted Intervention (MICCAI)*, volume 9351 of *LNCS*, pages 234–241, Munich, Germany, 2015. Springer.
- W. Samek, A. Binder, G. Montavon, S. Lapuschkin, and K.-R. Müller. Evaluating the visualization of what a deep neural network has learned. *IEEE Transactions on Neural Networks and Learning Systems*, 28:2660–2673, 11 2017. doi: 10.1109/TNNLS.2016.2599820.
- W. Samek, G. Montavon, S. Lapuschkin, C. J. Anders, and K.-R. Müller. Explaining deep neural networks and beyond: A review of methods and applications. *Proc. of the IEEE*, 109(3):247–278, 2021.
- U. Schlegel, H. Arnout, M. El-Assady, D. Oelke, and D. Keim. Towards a rigorous evaluation of xai methods on time series. *IEEE/CVF Intl. Conf. on Computer Vision Workshop (ICCVW)*, pages 4197–4201, 2019.
- L. M. Schmidt, G. Kontes, A. Plinge, and C. Mutschler. Can you trust your autonomous car? interpretable and verifiably safe reinforcement learning. In *IEEE Intelligent Vehicles Symposium (IV)*, pages 171–178, Tokyo, Japan, 2021.
- M. Schuster and K. Paliwal. Bidirectional recurrent neural networks. *IEEE Transactions on Signal Processing*, 45(11):2673–2681, 1997.
- R. R. Selvaraju, M. Cogswell, A. Das, R. Vedantam, D. Parikh, and D. Batra. Grad-cam: Visual explanations from deep networks via gradient-based localization. In *IEEE Intl. Conf. on Computer Vision*, pages 618–626, Venice, Italy, 2017.
- W. Silva, K. Fernandes, M. J. Cardoso, and J. S. Cardoso. Towards Complementary Explanations Using Deep Neural Networks. In D. Stoyanov, Z. Taylor, S. M. Kia, I. Oguz, M. Reyes, A. Martel, L. Maier-Hein, A. F. Marquand, E. Duchesnay, T. Löffstedt, B. Landman, M. J. Cardoso, C. A. Silva, S. Pereira, and R. Meier, editors, *Understanding and Interpreting Machine Learning in Medical Image Computing Applications*, volume 11038, pages 133–140. Springer International Publishing, Cham, Switzerland, 2018. doi: 10.1007/978-3-030-02628-8_15.
- K. Simonyan, A. Vedaldi, and A. Zisserman. Deep inside convolutional networks: Visualising image classification models and saliency maps. *arXiv preprint arXiv:1312.6034*, 2014.

- D. Smilkov, N. Thorat, B. Kim, F. Viégas, and M. Wattenberg. Smoothgrad: removing noise by adding noise. *arXiv preprint arXiv:1706.03825*, 2017.
- J. T. Springenberg, A. Dosovitskiy, T. Brox, and M. A. Riedmiller. Striving for simplicity: The all convolutional net. In Y. Bengio and Y. LeCun, editors, *3rd International Conference on Learning Representations, ICLR 2015*, San Diego, CA, 2015.
- N. Srivastava, G. Hinton, A. Krizhevsky, I. Sutskever, and R. Salakhutdinov. Dropout: A simple way to prevent neural networks from overfitting. *J. Mach. Learn. Res.*, 15(1): 1929–1958, Jan. 2014. ISSN 1532-4435.
- N. Strodthoff and C. Strodthoff. Detecting and interpreting myocardial infarction using fully convolutional neural networks. *Physiological Measurement*, 40(1):015001, jan 2019.
- M. Sundararajan, A. Taly, and Q. Yan. Axiomatic attribution for deep networks. In *International Conference on Machine Learning*, pages 3319–3328, Sydney, Australia, 2017. PMLR.
- N. Tatbul, T. J. Lee, S. Zdonik, M. Alam, and J. Gottschlich. Precision and recall for time series. In *Advances in Neural Information Processing Systems*, volume 31, Montréal, Canada, 2018. Curran Associates, Inc.
- R. Tomsett, D. Harborne, S. Chakraborty, P. Gurram, and A. Preece. Sanity Checks for Saliency Metrics. In *Proceedings of the AAAI Conference on Artificial Intelligence*, volume 34, pages 6021–6029, 2020. doi: 10.1609/aaai.v34i04.6064.
- T. K. Vintsyuk. Speech discrimination by dynamic programming. *Cybernetics*, 4(1):52–57, 1968.
- Z. Wang, A. C. Bovik, H. R. Sheikh, and E. P. Simoncelli. Image quality assessment: from error visibility to structural similarity. *IEEE Transactions on Image Processing*, 13(4): 600–612, 2004.
- Z. Wang, W. Yan, and T. Oates. Time series classification from scratch with deep neural networks: A strong baseline. In *Intl. Joint Conf. on Neural Networks*, pages 1578–1585, Anchorage, AK, 2017.
- A. Warnecke, D. Arp, C. Wressnegger, and K. Rieck. Evaluating explanation methods for deep learning in security. In *IEEE European Symposium on Security and Privacy, EuroS&P*, pages 158–174, Genova, Italy, 2020.
- C.-K. Yeh, C.-Y. Hsieh, A. S. Suggala, D. I. Inouye, and P. Ravikumar. On the (In)fidelity and Sensitivity of Explanations. In *Advances in Neural Information Processing Systems*, page 12, Vancouver, Canada, 2019. Curran Associates, Inc.
- G. Yona and D. Greenfeld. Revisiting Sanity Checks for Saliency Maps. In *Workshop on eXplainable AI Approaches for Debugging and Diagnosis at NeurIPS*, page 10, Vancouver, Canada, 2021.

- H. Zhang, Y. Yu, J. Jiao, E. P. Xing, L. E. Ghaoui, and M. I. Jordan. Theoretically principled trade-off between robustness and accuracy. In K. Chaudhuri and R. Salakhutdinov, editors, *Proceedings of the 36th International Conference on Machine Learning, ICML 2019, 9-15 June 2019, Long Beach, California, USA*, volume 97 of *Proceedings of Machine Learning Research*, pages 7472–7482, Long Beach, CA, 2019. PMLR.
- Q. Zhang and S. Zhu. Visual interpretability for deep learning: a survey. *Frontiers Inf. Technol. Electron. Eng.*, 19(1):27–39, 2018.
- B. Zhou, A. Khosla, A. Lapedriza, A. Oliva, and A. Torralba. Learning deep features for discriminative localization. In *Proceedings of the IEEE Conference on Computer Vision and Pattern Recognition (CVPR)*, Las Vegas, NV, June 2016.